High metabolic zinc demand within native Amundsen and Ross Sea phytoplankton communities determined by stable isotope uptake rate measurements

Riss M. Kell[1,+], Rebecca J. Chmiel[1], Deepa Rao[1], Dawn M. Moran[1], Matthew R. McIlvin[1], Tristan J. Horner[1], Nicole L. Schanke[3], Ichiko Sugiyama[1], Robert B. Dunbar[2], Giacomo R. DiTullio[3], Mak A. Saito[1]

[1]Department of Marine Chemistry and Geochemistry, Woods Hole Oceanographic Institution, Woods Hole, MA, USA

[2]Doerr School of Sustainability, Stanford University, Stanford, CA 94305

[3]Hollings Marine Laboratory, College of Charleston, Charleston, South Carolina, 29412, USA

Correspondence to: Mak A. Saito (msaito@whoi.edu)

[+]Formerly published under Riss Kellogg; now affiliated with Gloucester Marine Genomics Institute, Gloucester MA, 01930-3006

Abstract. Zinc (Zn) is an essential micronutrient for most eukaryotic phytoplankton. Zn uptake by phytoplankton within the euphotic zone results in nutrient-like dissolved Zn (dZn) profiles with a large dynamic range. The combination of key biochemical uses for Zn and large vertical gradients in dZn implies the potential for rapid rates of Zn removal from the surface ocean. However, due to the ease of contamination at sea, direct measurements of dZn uptake within natural environments have not been previously made. To investigate the demand for dZn and for dissolved cadmium (dCd; a closely related nutrient-like element) within Southern Ocean phytoplankton communities, we conducted ^{67}Zn and ^{110}Cd tracer uptake experiments within the Amundsen Sea, Ross Sea, and Terra Nova Bay of the Southern Ocean. We observed a high magnitude of Zn uptake (ρZn > 100 pmol dZn L^{-1} d^{-1}) into the particulate phase that was consistent with ambient depleted dZn surface concentrations. High biomass and low seawater

pCO_2 appeared to contribute to ρZn, which also led to increases in ρCd likely through the upregulation of shared transport systems. These high ρZn measurements further imply that only short timescales are needed to deplete the large winter dZn inventory down to the observed surface levels in this important carbon-capturing region. Overall, the high magnitude of Zn uptake into the particulate fraction suggests that even in the Zn-rich waters of the Southern Ocean, high Zn uptake rates can lead to Zn depletion and potential Zn scarcity.

1 Introduction

Zinc (Zn) is an essential trace metal micronutrient for marine phytoplankton with roles in carbon fixation, organic phosphorus uptake, and transcriptional and translational processes, among others (Morel et al., 2013, 2020; Shaked et al., 2006; Twining and Baines, 2013). Nutrient-like depth profiles of total dissolved Zn (dZn) are characterized by depleted surface concentrations due to uptake by phytoplankton within the euphotic zone, reflecting this high biological demand (Fitzwater et al., 2000; Lohan et al., 2002; Middag et al., 2019; Zhao et al., 2014). Zn is particularly important as a catalytic cofactor in carbonic anhydrase (CA) metalloenzymes, which catalyze the reversible dehydration of HCO_3^- to CO_2. As HCO_3^- constitutes about 90% of the dissolved inorganic carbon (DIC) pool in the surface ocean, CAs in marine algae are a critical part of the carbon concentrating mechanism (CCM) that maintains a CO_2 supply to the carbon-fixing enzyme ribulose-1,5-biphosphate carboxylase/oxygenase (RUBISCO). Less abundant divalent metal cations such as cobalt (Co^{2+}) and cadmium (Cd^{2+}) can replace Zn^{2+} in some algal CA subtypes (Lane et al., 2005), conferring biochemical flexibility to algae confronted with low Zn bioavailability.

While Cd is known to cause toxic effects in most organisms (Brand et al., 1986; Das et al., 1997), dCd depth profiles are also nutrient-like. As noted above, the biological use of Cd as a

47 catalytic cofactor within Cd-containing carbonic anhydrase (ζ-CA, or CDCA) likely contributes
48 to surface dCd depletion and thus to the observed nutrient-like profiles, though this remains the
49 only known biological use of Cd to date (Haas et al., 2009; Lee and Morel, 1995; Sunda and
50 Huntsman, 2000). It has also been proposed that phytoplankton may assimilate Cd abiotically—
51 this mode of Cd uptake is non-specific, a case of 'mistaken identity' in which phytoplankton
52 bind and store imported Cd inside the cell to avoid toxicity, coupling the cycling of Cd to the
53 biological cycle of nutrients (Horner et al., 2013). As the beneficial effect of adding Cd to
54 phytoplankton cultures has only been observed when Zn is limiting (Lee et al., 1995; Price and
55 Morel, 1990; Xu et al., 2007), it has been speculated that the ability to use Cd in place of Zn in
56 CDCA may confer a competitive advantage to Zn-limited algae under low pCO_2. To date,
57 homolog *cdca* genes have been found exclusively in diatom species (Park et al., 2007, 2008).
58 However, since the beneficial effect of Cd has also been observed in organisms such as the green
59 alga *Tetraselmis maculata* and the coccolithophore *Emiliania huxleyi* that lack the *cdca* gene
60 (Lee and Morel, 1995), it is thought that Cd may have other biochemical functions in
61 phytoplankton still awaiting discovery.
62 Due to the generally high (> 1nM) dZn concentrations observed in Southern Ocean
63 waters (Baars and Croot, 2011), Zn has not been considered to be a limiting micronutrient in this
64 region, despite the fact that Southern Ocean diatom species possess cellular Zn quotas that are 3-
65 15x higher compared to those of low-latitude species (Twining and Baines, 2013), with model-
66 inferred Zn uptake rates used to find that Southern Ocean phytoplankton account for 62% of
67 global Zn uptake (Roshan et al., 2018). Substantial removal of dZn from Southern Ocean surface
68 waters appears associated with high biomass blooms and low pCO_2 conditions during austral
69 spring and summer, creating the potential for phytoplankton growth to become Zn and carbon

co-limited (Kell et al., 2023; Morel et al., 1994). While phytoplankton growth in the Southern Ocean is well-known to be primarily limited by Fe availability (Arrigo et al., 2008; Martin, 1990), melting icebergs and ice shelves are known to act as external sources of Fe (Hopwood et al., 2019; Person et al., 2021; Planquette et al., 2013; St-Laurent et al., 2017) with larger Fe inputs expected from increased ice melt in a warming climate. The majority of ice-melted Fe input is sourced from particulate lithogenic material (entrained during grounding of ice shelves on the continent and sediments). Fe in crustal material is more abundant than Zn (3.5% as Fe versus 0.0071% as Zn) (Taylor and McLennan, 1985), creating a large inventory of particulate Fe available that can be partially dissolved by biotic and abiotic processes. Increased dFe inputs to surface Antarctic waters may act to relieve Fe stress, but would simultaneously support the development of other nutrient limitations. For example, low availabilities of both dZn and vitamin B_{12} have been previously observed to co-limit phytoplankton growth with Fe in the Ross Sea (Bertrand et al., 2007; Kell et al., 2023). A high demand for Zn naturally exists within eukaryotic phytoplankton due to the requirement for Zn^{2+} in numerous metabolic functions; therefore, without similarly enhanced inputs of dZn to the water column, the alleviation of primary Fe limitation could induce Zn stress as the next most in-demand metal micronutrient. Coastal polynyas that form within the Amundsen and Ross Seas during austral spring and summer are particularly primed to experience Zn stress as these regions host highly productive seasonal phytoplankton blooms that act as significant carbon sinks (Arrigo et al., 2012). This high productivity draws pCO_2 down to low levels (< 200 ppm), putting pressure on the carbon concentrating mechanism of photosynthetic phytoplankton to acquire CO_2 and thus to acquire Zn as the predominantly utilized metal cofactor within carbonic anhydrases.

The present study enhances our knowledge of the rate of dZn removal from the surface Southern Ocean and uptake into the particulate fraction with empirical field data measured within native Southern Ocean phytoplankton communities. This study developed a field-based, stable Zn isotope uptake rate method, building on a prior stable Cd uptake rate method (Cox et al., 2014). While Zn uptake has been measured in laboratory cultures (Sunda and Huntsman, 1992, 1995, 2000), and the influence of grazing and tropic transfer studies have been conducted using radioactive isotopes (Hutchins and Bruland, 1995, 1994), to our knowledge direct measurements of Zn uptake in natural marine phytoplankton communities have not been conducted previously, despite interest in modeling the biogeochemical uptake and cycling of Zn (Weber et al., 2018). We measured the total uptake rates of Zn and Cd along the shelves of the Amundsen Sea and Ross Sea during the austral summer of 2017-2018 (December – March). This was accomplished by introducing ^{67}Zn and ^{110}Cd (with natural abundances of 4.10% and 12.5%, respectively) into short-term (24 hr) incubation experiments. The aim was to quantify the transfer of dissolved $^{110}Cd^{2+}$ and $^{67}Zn^{2+}$ into the particulate fraction exceeding 3 μm. Both stable isotopes can be used as uptake tracers by analysis of isotope abundances that deviate from natural abundances within the particulate phase. The transfer of added isotopes into the particulate phase is the combined result of 1) active transport of metal into cells, 2) nonspecific metal adsorption to cell surfaces, 3) metal adsorption to non-living particulate organic matter, and 4) metal adsorption to particulate inorganic matter, though we expect active transport into cells to dominate the measured particulate isotopic signal due to the high abundance of actively growing autotrophic cells in the photic zone observed in the Southern Ocean during austral summer. These measurements of uptake rates were then used to infer timescales of surface dZn depletion in these Antarctic environments. These uptake rates contribute to understanding the biological

demand and potential for Zn limitation of primary productivity in highly productive coastal environments, such as the polynyas surrounding Antarctica (Kell et al., 2023).

2 Methods

2.1 Study area and sample collection

Samples were collected during the CICLOPS (Cobalamin and Iron Co-Limitation of Phytoplankton Species) expedition (NBP18-01) aboard the RVIB *Nathaniel B. Palmer*, December 11, 2017 – March 3, 2018 in the Amundsen Sea and Ross Sea of the Southern Ocean (Fig. 1).

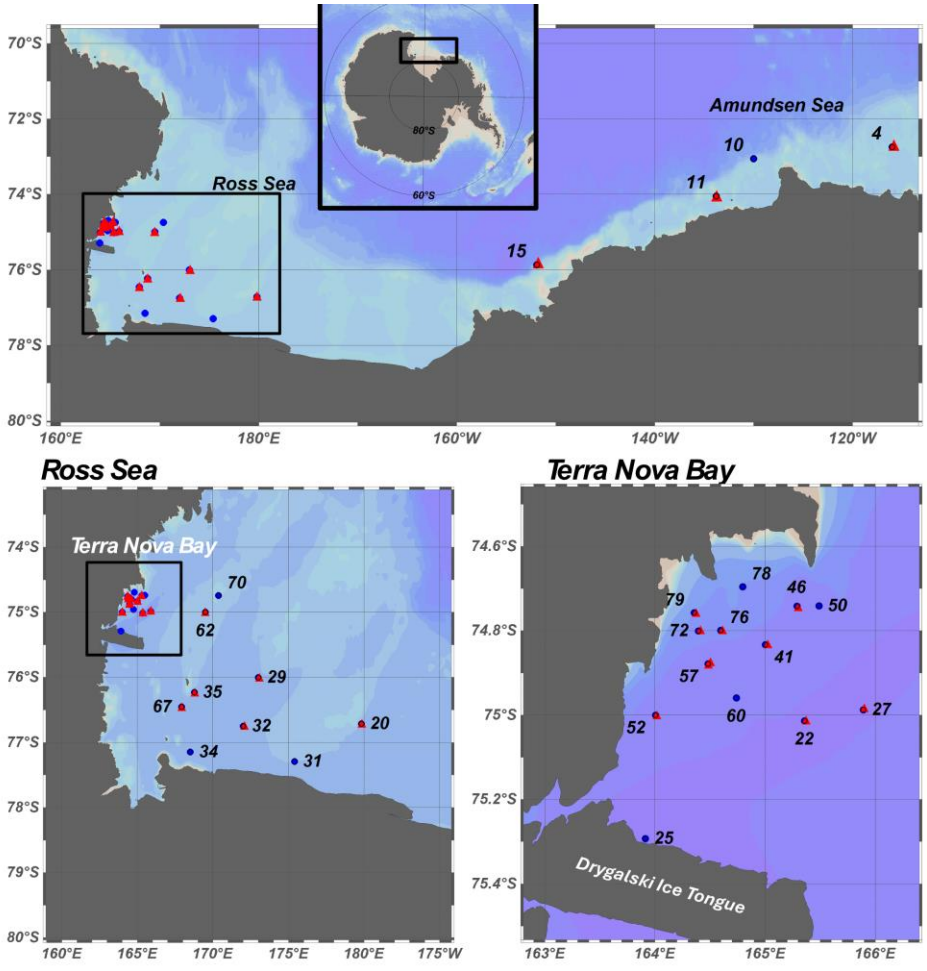

Figure 1. Map showing the stations sampled over the course of the CICLOPS cruise. Stations marked by red triangles indicate those at which stable ^{67}Zn and ^{110}Cd uptake rate experiments were performed. An expanded map of stations sampled in the Ross Sea is shown at bottom left, while a further expansion of stations sampled in Terra Nova Bay is shown at bottom right.

Station metadata is given in Table S1. Water samples were collected using trace metal clean (TMC) sampling protocols described previously (Cutter and Bruland, 2012). A TMC rosette suspended on a Kevlar line and equipped with twelve 8L X-Niskin bottles (Ocean Test Equipment) was used to collect seawater at depths ranging from 10 – 600 m. Continuous underway measurements of pCO_2 at ~5 m depth were taken using a pCO_2 measurement system from Lamont-Doherty Earth Observatory (LDEO, 0.017/sec rate). Hydrography data were collected using sensors deployed on a titanium trace metal rosette (TMR) in tandem with TMC niskin bottles. The TMR was equipped with sensors to measure temperature, conductivity, pressure, dissolved oxygen, chlorophyll (Chl) fluorescence, altimetry, beam transmission, and photosynthetically active irradiance (PAR). Chl fluorescence was measured using a WetLabs ECO-FL fluorometer. A complete data report and sensor list are available at NBP1801DATA.pdf (rvdata.us). Mixed layer depth (MLD) was determined for each station within Terra Nova Bay as the first depth at which the difference between the potential density (σ_θ) and reference density (the potential density at 10m, σ_{ref}) was greater than or equal to 0.125 kg m^{-3} (Bishop and Wood, 2009; Ohnemus et al., 2017).

2.2 Preparation of plasticware

Polyethylene and polycarbonate sampling and incubation bottles were rigorously cleaned to remove trace metal contaminants before use. Bottles with rinsed with Milli-Q water (Millipore), soaked for 72h in <1% Citranox detergent, rotated, soaked for an additional 72h, and then rinsed five times with Milli-Q water. Bottles were then filled with 10% HCl (Baker instra-

analyzed) by volume and soaked for a minimum of one week, rotated, and soaked for another week. Bottles were then rinsed five times with dilute acid (HCl, pH 2) and stored double-bagged in plastic zip bags. All cleaning work was conducted in a Class 100 clean room. Polypropylene 15 mL centrifuge tubes used in sample processing were cleaned of potential metal contamination by soaking in 10% HCl for 5 days and rinsing with pH 2 HCl prior to use.

2.3 Sampling for total dissolved metal analyses

Samples for the analysis of total dissolved Zn, Cd, Fe, Mn, Cu and Ni concentrations were collected shipboard by pressure-filtering X-Niskin bottles through an acid-washed 142mm, 0.2µM Supor membrane filter (Pall) within 3 hours of rosette recovery using high purity (99.999%) N_2 gas. Total dissolved water samples were collected into 250 mL TMC polyethylene bottles and stored double-bagged in plastic zip bags. Seawater samples for ^{110}Cd and ^{67}Zn stable isotope uptake experiments were collected in the same way but without filtering. All sample collection occurred shipboard within a TMC van containing laminar flow hoods and plastic sheeting. Samples for total dissolved metal analysis were acidified to pH 1.7 with high purity HCl (Optima, Fisher Scientific) within 7 months of sampling and were stored acidified at room temperature for over 1 year prior to analysis.

2.4 Analyses of total dissolved metals using isotope dilution

Quantification of dissolved metals in samples and reference seawater was performed for total dissolved Fe, Ni, Cu, Zn, and Cd using isotope dilution. 15 mL of acidified seawater sample was spiked with 50 µL of a stable isotope spike solution artificially enriched in ^{57}Fe, ^{61}Ni, ^{65}Cu, ^{67}Zn, and ^{110}Cd ('spike isotopes'). Reference isotopes used in this study were ^{56}Fe, ^{60}Ni, ^{63}Cu, ^{66}Zn, and ^{114}Cd. All spike isotopes were received in solid form (Oak Ridge National Laboratory). Initial dissolution and all subsequent dilutions were made using concentrated nitric

acid (Optima, Fisher Scientific). Concentrations and ratios of isotopes for each metal in the spike solution were verified by inductively coupled plasma mass spectrometry (ICP-MS) using a multi-element standard curve (SPEX CertiPrep). The composition of the isotope spike addition was made such that the target isotope ratios in the total, 15mL spiked sample would be $^{57}Fe/^{56}Fe$ = 0.7, $^{61}Ni/^{60}Ni$ = 0.5, $^{65}Cu/^{63}Cu$ = 1, $^{67}Zn/^{66}Zn$ = 0.7, and $^{110}Cd/^{114}Cd$ = 1 and were verified with ICP-MS. These ratios were chosen to minimize the uncertainty introduced by error propagation through the isotope dilution equation (Kato et al., 1990; Rudge et al., 2009; Tan et al., 2020; Wu and Boyle, 1998). The same spike solution was used to spike all samples from all depths. Because it is monoisotopic, total dissolved Mn was calculated using a modified isotope dilution equation:

$$\mathrm{Mn\ (nM)} = \frac{^{55}\mathrm{Mn_{spl}\ (cps)}}{^{57}\mathrm{Fe_{spl}\ (cps)}} * {}^{57}\mathrm{Fe_{spike}\ (nM)} * {}^{57}\mathrm{Fe_{slope}\ (cps/ppb)} * \frac{1}{(^{55}\mathrm{Mn_{slope}})\ \mathrm{(cps/ppb)}} \qquad (1)$$

in which $^{55}Mn_{spl}$ and $^{57}Fe_{spl}$ refer to the blank corrected counts per second (cps) of ^{55}Mn and ^{57}Fe in the spiked sample, ^{57}Fe spike is the concentration of ^{57}Fe in the spike, $^{57}Fe_{slope}$ is the slope of the external standard calibration curve (SPEX curve) relating ^{57}Fe cps to ppb, and $^{55}Mn_{slope}$ is the slope of the external calibration curve (SPEX curve) relating ^{55}Mn cps to ppb. Due to the acidification of seawater prior to ICP-MS analysis, Mn ICP-MS measurements do not include contributions from humic-type Mn(III)-ligand complexes (Oldham et al., 2021). Until the inclusion of Mn(III) is resolved and intercalibrated, we report these Mn values as Mn(II) and note that they are consistent with prior studies employing the same acidification technique (Gerringa et al., 2020; Noble et al., 2013; Sedwick et al., 2000).

Preconcentration of spiked seawater samples for total dissolved metal analysis was performed using the automated solid phase extraction system seaFAST-pico (Elemental Scientific) in offline concentration mode with an initial volume of 15 mL and elution volume of

500 µL (Bown et al., 2017; Jackson et al., 2018; Rapp et al., 2017; Wuttig et al., 2019). The seaFAST contains a Nobias-chelate PA1 resin column (ethylenediaminetriacete and iminodiacetate) suitable for the simultaneous preconcentration of several trace metals (Fe, Mn, Zn, Cu, Co, Cd, Ni) with high sensitivity and quantitative recovery (Biller and Bruland, 2012; Sohrin et al., 2008). Adjusted seaFAST software settings were a 17 second load loop time and a single 10 mL load cycle.

Reagents consisted of a 1.5M ammonium acetate pH 6.0 buffer made using glacial acetic acid and ammonium hydroxide (20-22%) of the highest purity (Optima, Fisher Chemical), a 1% nitric acid rinse solution (Optima grade, Fisher Chemical), and a 10% nitric acid elution buffer (Optima grade, Fisher Chemical) with 10 ppb indium (^{115}In, SPEX CertiPrep) added as an internal standard. Solutions were prepared with 18.2 Ω Milli-Q water (Millipore).

Following offline seaFAST preconcentration, multi-elemental quantitative analysis was performed using an iCAP-Q inductively coupled plasma-mass spectrometer (Thermo Scientific). To minimize oxide interference on metal isotopes, a cooled spray chamber and helium collision gas were employed. Analytes were measured in single quadruple mode (kinetic energy discrimination [KED]). Concentrations of Mn, Fe, Ni, Cu, Zn and Cd were determined using a six-point external standard curve of a multi-element standard (SPEX CertiPrep), diluted to range from 1-10 ppb in 5% nitric acid. An indium standard (SPEX CertiPrep) was similarly added to these standard stocks, diluted to range 1-10 ppb. Instrument injection blanks consisted of 5% nitric acid in Milli-Q. Standard curve R^2 values were ≥ 0.98 for all metals monitored. Method accuracy and precision were assessed using the 2009 GEOTRACES coastal surface seawater (GSC) standard (n = 8; Table S2), which produced values consistent with consensus results.

2.5 Procedural blanks and limit of detection (LOD).

Procedural blanks were quantified by preconcentrating 30mL of MilliQ water adjusted to pH 2 with HCl (Optima, Fisher Scientific) to 1mL. Metal concentrations were determined using an external SPEX multi-element standard as described above. The LOD was calculated as 3 x the standard deviation of the blank measurements (13.5 pM Fe, 2.9 pM Ni, 1.6 pM Cu, 38.1 pM Zn, and 0.3 pM Cd).

2.6 Uptake experiments: ^{67}Zn and ^{110}Cd spiking, incubation, and sample collection

^{67}Zn and ^{110}Cd and stable isotope uptake experiments were modeled after those conducted by Cox et. al. 2014, with the addition of Zn uptake measurements. An overall schematic detailing these experiment workflows is shown in Fig. 2.

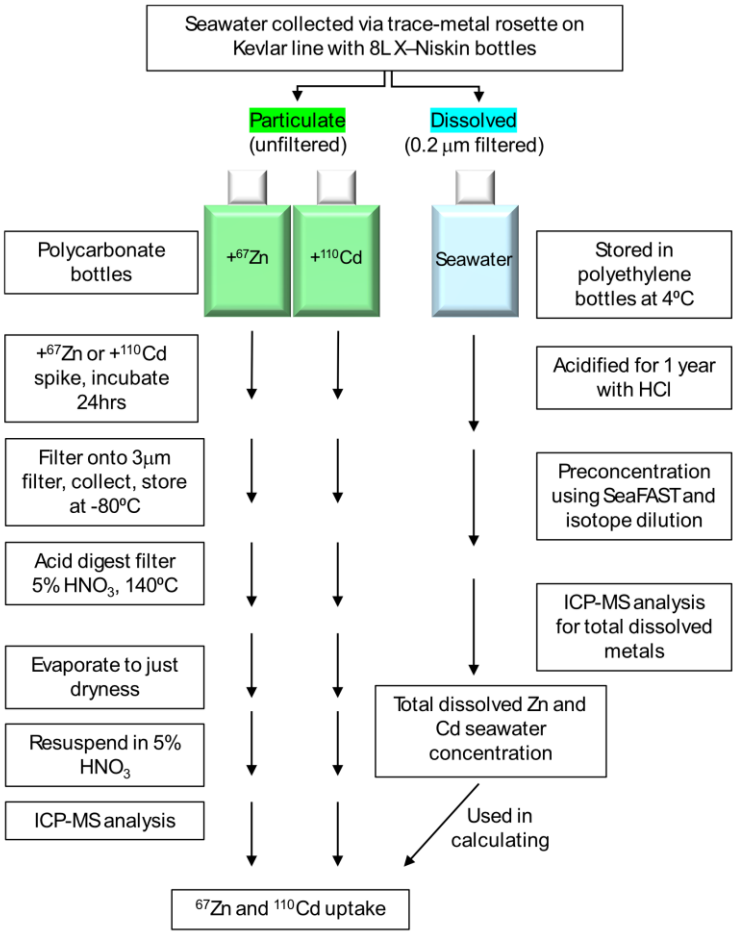

Figure 2. Diagram showing the overall workflow used to measure particulate uptake of ^{110}Cd and ^{67}Zn and total dissolved Cd and Zn, after Cox et al. 2014.

Uptake experiments were performed at 18 stations total (Fig. 1). Raw (unfiltered) seawater was collected shipboard over a depth range of 10 – 600 m into 250 mL TMC polycarbonate incubation bottles. All incubation bottles were filled with minimal headspace such that the total culture volume was ~275 mL. Two incubation bottles per depth were filled with raw seawater—one was spiked with ^{67}Zn, the other was spiked with ^{110}Cd. The Cd and Zn isotope spikes were prepared by dissolving ^{110}CdO and ^{67}ZnO (Oak Ridge National Laboratory) in 5% HNO_3 (Seastar Baseline) and were diluted using Milli-Q water to minimize added acidity. When added to the filled incubation bottles, the total added (spiked) concentration of Cd was 300 pM and the total added concentration of Zn was 2 nM. The chosen total added concentrations were based on the surface ratio of total dissolved Cd (dCd) to total dissolved Zn (dZn) reported previously for the Ross Sea (Fitzwater et al., 2000). Immediately after spiking, incubation bottles were sealed, inverted to mix, and transferred to flow-through on-deck incubators for 24hr. Incubators were shielded by black net neutral density screening to allow 20% ambient light penetration.

Biomass was collected after 24hr by vacuum filtering the entire volume of each incubation sample at 34.5 kPa (5 psi) onto an acid-cleaned 3μm, 50mm acrylic copolymer (Versapore) filter (Pall) mounted on an acid-cleaned Teflon (Savillex) filtration rig. Samples were filtered through 3 μm pore-size filters rather than 0.2 μm in order to minimize filtration time (and thus time exposed to potential contamination) and to capture the bulk of eukaryotic phytoplankton biomass typically found in the Southern Ocean. An aliquot of 1 mL of 0.2 μm filtered surface seawater (collected at 10 m depth) was used to rinse the sample before collecting the filter into an acid-cleaned 2 mL cryovial using acid-rinsed plastic forceps. Filter blanks were

duplicate 3 μm acid-clean Versapore (Pall) filters that were placed onto the filtration rig, rinsed with filtered surface seawater, collected, stored, and processed as samples were to correct for any contaminating metals present on the filters themselves. Blanks were collected at each station. Filters were stored frozen at -80ºC in acid-cleaned cryovials until analysis. The filtration rig was rinsed with pH 2 HCl between samples. Polycarbonate incubation bottles were cleaned between stations with a 10% HCl rinse and several rinses in Milli-Q water, followed by a brief soak in 10% HCl followed by a pH 2 HCl rinse. All spike addition and sample filtration procedures were completed in a fabricated shipboard positive-pressure clean room environment made of laminar flow hoods and plastic sheeting.

We note that the total Zn and Cd uptake rate values presented in this study represent potential uptake rates rather than true uptake rates—this naturally arises as a consequence of adding the spiked tracer ^{67}Zn and ^{110}Cd into raw surface seawater. As this seawater is naturally depleted in both metals, the spike addition artificially increases the total Zn and Cd present and thus could perturb the response of biology to these additions. It should also be noted that both ^{67}Zn and ^{110}Cd spikes were not equilibrated with natural seawater before their addition to incubation bottles to maintain experimental consistency. Experiments of this nature have been conducted previously using radioisotopes as tracers (Cullen et al., 1999; Hutchins et al., 1999; Morel et al., 1994; Sunda and Huntsman, 1995), though we chose to use stable isotopes for ease of shipboard use and waste disposal.

2.7 Filter digestion and particulate ICP-MS analysis

All work was performed in a Class 100 clean room under laminar flow hoods. Sample filters were retrieved from storage at -80ºC, removed from cryovials using plastic acid-washed forceps, and transferred into trace metal clean 15 mL PFA vials with 4 mL of 5% HNO_3

(Optima) containing a 1 ppb Indium (In) internal standard. Filters were digested for ~3.5h at 140ºC using a HotBlock® heating block (Environmental Express, USA). Filters were then removed and discarded, leaving behind the liquid extract. After evaporating the remaining solution to just dryness, the residue was resuspended in 2 mL of 5% HNO_3 (Optima) by light vortexing. Process blank filters were digested and processed as sample filters were. Digests were analyzed in duplicate by ICP-MS using a Thermo ICAP-Q plasma mass spectrometer calibrated to a multi-element standard curve (SPEX Certiprep) over a range of 1 – 20 ppb. Duplicate values were in good agreement (Supplementary File 1), and the average value was used in further calculations. Natural Cd and Zn isotope abundances of the standards were assumed to calculate concentrations of ^{110}Cd, ^{111}Cd, ^{114}Cd, ^{67}Zn, ^{66}Zn, and ^{68}Zn. Digests were analyzed in KED mode after an 85s sample uptake window and element mass windows were scanned 3 times during measurements. The 1 ppb In internal standard was used to correct for variation in sample delivery and plasma suppression between samples. Process blanks were subtracted from measured sample concentrations. Phosphorus concentrations were simultaneously measured by ICP-MS and were calibrated to a standard curve ranging from 100 – 3,200 ppb using a 1 ppm certified P stock (Alfa Aesar Specpure). Equation #2 was used for the calculations described above:

$$M_{particulate} = \left[\frac{M_{sample}}{In_{sample}} - \frac{M_{blank}}{In_{blank}}\right] * \frac{In_{digestion}}{M_{slope}} * \frac{V_{digested}}{V_{filtered}} \quad (2)$$

where V_{filtered} is the total spiked sample volume estimated to have passed through the filter (275 mL), V_{digested} is the final volume the sample was resuspended in (2.0 mL), M_{sample} is the metal of interest measured in the sample in units of counts per second (cps), M_{blank} is the metal of interest measured in the process blanks (cps), M_{slope} is the slope of the metal of interest obtained by the standard curve (cps ppb^{-1}), In_{sample} is the In measured in the sample (cps), In_{blank} is the In

measured in the process blanks (cps), $In_{digestion}$ is the cps of In measured in the 5% HNO_3+1 ppb In digestion solution, and the calculated concentration of the metal of interest ($M_{particulate}$) is in ppb (μg L^{-1}). This equation is the same as that used by Noble et. al. 2013 for the determination of particulate metal concentrations using ICP-MS (Noble et al., 2013).

The Zn spike and Cd spike were also analyzed by ICP-MS using a tenfold dilution of spike solution into 5% HNO_3 containing 1 ppb In to determine isotopic compositions and concentrations. When added to filled incubation bottles (275 mL total volume), the added concentrations were 288 pM ^{110}Cd, 4.51 pM ^{111}Cd, and 1.69 pM ^{114}Cd for Cd spiked bottles, and were 1.91 nM ^{67}Zn, 0.045 nM ^{66}Zn, and 0.047 nM ^{68}Zn for Zn spiked bottles (Table S3). For all stations and all depths, ^{67}Zn and ^{110}Cd spike concentrations exceeded natural dissolved ^{67}Zn and ^{110}Cd concentrations, estimated by multiplying the total dissolved Zn and Cd by the natural isotope abundance of ^{67}Zn and ^{110}Cd (0.0410 and 0.1249, respectively; see comparisons in Fig. S2).

2.8 Calculating zinc and cadmium uptake using ^{67}Zn and ^{110}Cd

Total Zn and Cd uptake was calculated using Eq. (3) and Eq. (4), respectively. $^{110}Cd_{Sample}$ and $^{67}Zn_{Sample}$ are the particulate ^{110}Cd and ^{67}Zn measured by ICP-MS analysis of the 3 μm sample filter (using the digestion protocol described in section 2.7) normalized to the total culture volume (275 mL) and 24 hr of incubation. $^{110}Cd_{Sample}$ and $^{67}Zn_{Sample}$ already in the particulate fraction (that is, the pCd and pZn that existed in the water column upon collection of the raw seawater samples) were accounted for by subtracting these pre-existing particulate ^{110}Cd and ^{67}Zn values,$^{110}Cd_{PEP}$ and $^{67}Zn_{PEP}$. The pre-existing particulate value for ^{110}Cd was obtained from incubation bottles that had Zn added, but no Cd spike. Likewise, the pre-existing particulate value for ^{67}Zn was obtained from incubation bottles that had Cd added, but no Zn spike. The

^{67}Zn spike solution was confirmed to contain virtually no ^{110}Cd, ^{111}Cd, nor ^{114}Cd. The ^{110}Cd spike was likewise confirmed to contain virtually no ^{67}Zn, ^{64}Zn, nor ^{66}Zn. As a result, we assumed that the added ^{67}Zn spike did not affect the pre-existing Cd, nor did the ^{110}Cd spike affect the pre-existing Zn. It is assumed that the pre-existing particulate blank was in steady state, i.e. that it represented the Cd or Zn already in the particulate fraction and that any possible natural uptake that could occur during incubation for 24 h was negligible. The total dissolved pool of each metal isotope (denominator of each equation) is the sum of the dissolved ^{110}Cd or ^{67}Zn added as the spike ($^{110}Cd_{Spike}$, $^{67}Zn_{Spike}$) plus the natural, pre-existing dissolved ^{110}Cd or ^{67}Zn that was in the raw seawater ($^{110}Cd_{Natural}$, $^{67}Zn_{Natural}$) collected at each depth. To calculate $^{110}Cd_{Natural}$ and $^{67}Zn_{Natural}$, the total dissolved Cd or Zn measured by isotope dilution-ICP-MS (Cd_{Total}, Zn_{Total}) was multiplied by the natural abundance of ^{110}Cd and ^{67}Zn (12.49% and 4.10%, respectively). Dividing the particulate ^{110}Cd and ^{67}Zn by the total dissolved ^{110}Cd and ^{67}Zn yields the fraction of these metal isotopes that moved from the dissolved pool to the particulate pool per day (equation 3 and equation 4, respectively):

$$Cd_{total}\ \text{Uptake Rate}\ (\text{pmol L}^{-1}\ \text{d}^{-1}) = \frac{[^{110}Cd_{Sample}\ (\text{pmol L}^{-1}\ \text{d}^{-1}) - {}^{110}Cd_{PEP}\ (\text{pmol L}^{-1}\ \text{d}^{-1})]}{[^{110}Cd_{Spike}\ (\text{pmol L}^{-1}) + {}^{110}Cd_{Natural}\ (\text{pmol L}^{-1})]} \times Cd_{total}\ (\text{pmol L}^{-1}) \quad (3)$$

$$Zn_{total}\ \text{Uptake Rate}\ (\text{pmol L}^{-1}\ \text{d}^{-1}) = \frac{[^{67}Zn_{Sample}\ (\text{pmol L}^{-1}\ \text{d}^{-1}) - {}^{67}Zn_{PEP}\ (\text{pmol L}^{-1}\ \text{d}^{-1})]}{[^{67}Zn_{Spike}\ (\text{pmol L}^{-1}) + {}^{67}Zn_{Natural}\ (\text{pmol L}^{-1})]} \times Zn_{total}\ (\text{pmol L}^{-1}) \quad (4)$$

2.9 Nutrient analyses

Seawater samples taken for macronutrient analysis were filtered through 0.2 μm Supor (Pall) membrane filters and frozen at sea in acid-washed 60-mL high-density polyethylene (HDPE) bottles until analysis. Nutrient analyses were conducted by nutrient autoanalyzer by Joe Jennings at Oregon State University using previously described methods (Noble et al., 2012).

2.10 Statistics and plotting

Dissolved ecological stoichiometries were obtained from the slopes of two-way (type II) least squares linear regressions performed using the script lsqfitma.m rewritten from MATLAB to Python by Rebecca Chmiel (https://github.com/rebecca-chmiel/GP15). A correlation matrix of various parameters measured during NBP18-01 was created with SciPy v1.5.2 using the 'scipy.stats.pearsonr' function, yielding Pearson correlation coefficients and p values that were visually represented using Seaborn v.0.11.1 and Matplotlib v3.3.2. Ocean sections were plotted using Ocean Data View v5.3.0 with gridded bathymetry file ETOPO1_2min. Outliers (see Data Availability) were excluded from ocean sectional plots. Mixed layer depth was calculated using the potential density function (pden) within the python-seawater module (v3.3.4). Depth-integrated uptake rates were calculated using the 'auc' function within the Scikit-learn (v0.23.2) Python library. Figures were made using matplotlib (v3.3.2), Ocean Data View (v5.5.2), Excel (2019), and RStudio (v1.3.1093). ODV color palettes (https://doi.org/10.5281/zenodo.1243862) are inverse 'roma' for trace metal and macronutrient concentrations, 'thermal' for Zn and Cd uptake rates, and 'algae' for total fluorescence (Crameri, 2023).

3 Results

3.1 Amundsen Sea

Zn and Cd uptake rate experiments were conducted at 18 stations. We define 3 groups of stations based on location: the Amundsen Sea, Ross Sea, and Terra Nova Bay (TNB) groups (Fig. 1). Uptake rates were assessed at 3 stations (4, 11 and 15) within the Amundsen Sea group, 6 stations (20, 29, 32, 35, 62, and 67) within the Ross Sea group, and 9 stations (22, 27, 41, 46, 52, 57, 72, 76 and 79) within the TNB group spanning ~10 – 250 m depth for a total of 18 stations and 125 samples. An overall schematic detailing these experiment workflows is shown in Fig. 2. The experimental design was validated by comparison of surface particulate ^{67}Zn:^{68}Zn

368 and ^{110}Cd:^{114}Cd ratios measured in spiked samples with natural abundance ratios. Samples
369 spiked with ^{67}Zn had particulate ^{67}Zn:^{68}Zn ratios larger than natural abundance ratios at all
370 stations (as was also true for ^{110}Cd spiked samples and Cd natural abundances; Fig. S1),
371 indicative of uptake of the spike into the particulate phase.

372 The Amundsen Sea stations represented a linear cruise track, and we report total
373 dissolved metal concentrations (dMetal$_T$) and uptake rates (ρMetal) over time in order of station
374 sampling date (Fig. 3a).

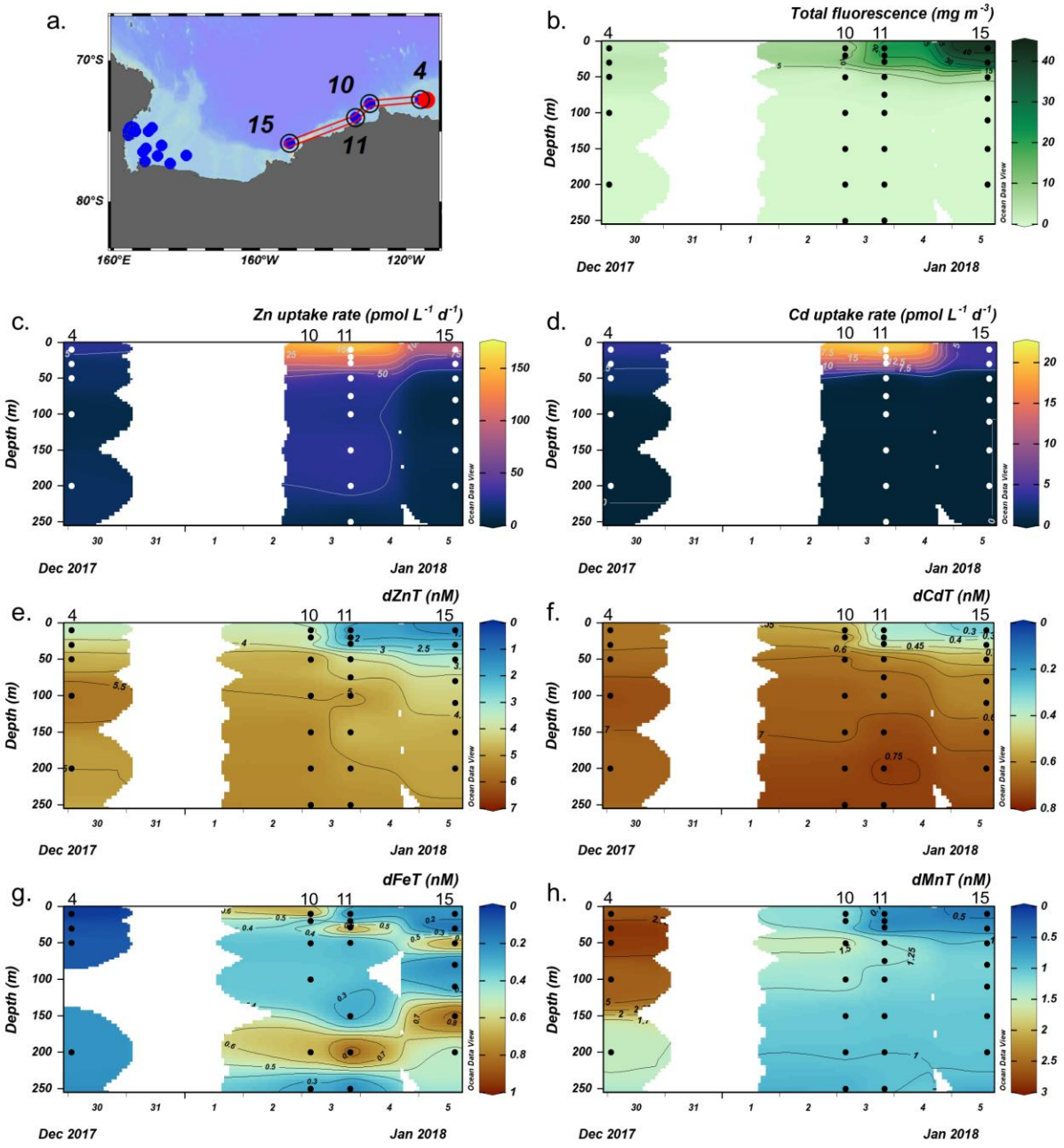

Figure 3. Total fluorescence and trace metal concentrations measured at Amundsen Sea stations shown over time. (a) Map showing station locations, (b) total chlorophyll (Chl) fluorescence, (c) total Zn uptake rates, (d) total Cd uptake rates, (e) total dissolved Zn, (f) total dissolved Cd, (g) total dissolved Fe, and (h) total dissolved Mn measured in the upper 250 m represented in color scale. Uptake experiments were not performed at station 10. Metal concentrations measured to 500 m depth are shown in Figure S3. dZnT, total dissolved Zn; dCdT, total dissolved Cd; dFeT, total dissolved Fe; dMnT, total dissolved Mn.

Among these stations, total Chl fluorescence was lowest at station 4 and increased moving westward along the transect to a Chl maximum of 41.8 mg m^{-3} at station 15, 10 m (Fig. 3b). Maximum surface concentrations of dZn, dCd and dMn were highest at station 4 (3.5 nM, 639 pM, and 2.6 nM at 10 m, respectively; Fig. 3e, f, h), likely reflecting the relatively smaller amount of total biomass (as indicated by total Chl fluorescence; Fig. 3b) at this station. Concentrations of dZn, dCd and dMn decreased moving westward along the transect (Fig. 3e, f, h) as total Chl fluorescence increased (Fig. 3b). Total Zn uptake rates (ρZn) and total Cd uptake rates (ρCd) were highest at station 11 (158 and 21 pmol L^{-1} d^{-1}, respectively, at 10 m; Fig. 3c,d; Fig. 4b). Among the three Amundsen Sea stations, the largest movement of both Zn and Cd into the particulate phase therefore occurred at station 11, concurrent with the relatively higher dFe_T surface values observed at station 11 (0.2 nM dFe compared to 0.01 nM at station 4, 10 m; Fig. 3g, Fig. S3c). The dFe concentrations exceeding 1 nM near the seafloor are consistent with a sedimentary or subglacial source (Fig. S3c). Overall, ρZn and ρCd profiles exhibited trends in which values were highest within the upper 50 m at all three stations and decreased with depth, following the trend in Chl a or total Chl fluoresence (Fig. 4). Vertical sections of dZn and dCd through the water column mirrored these trends (Fig. 4), demonstrating the movement of these dissolved metal micronutrients into the particulate phase.

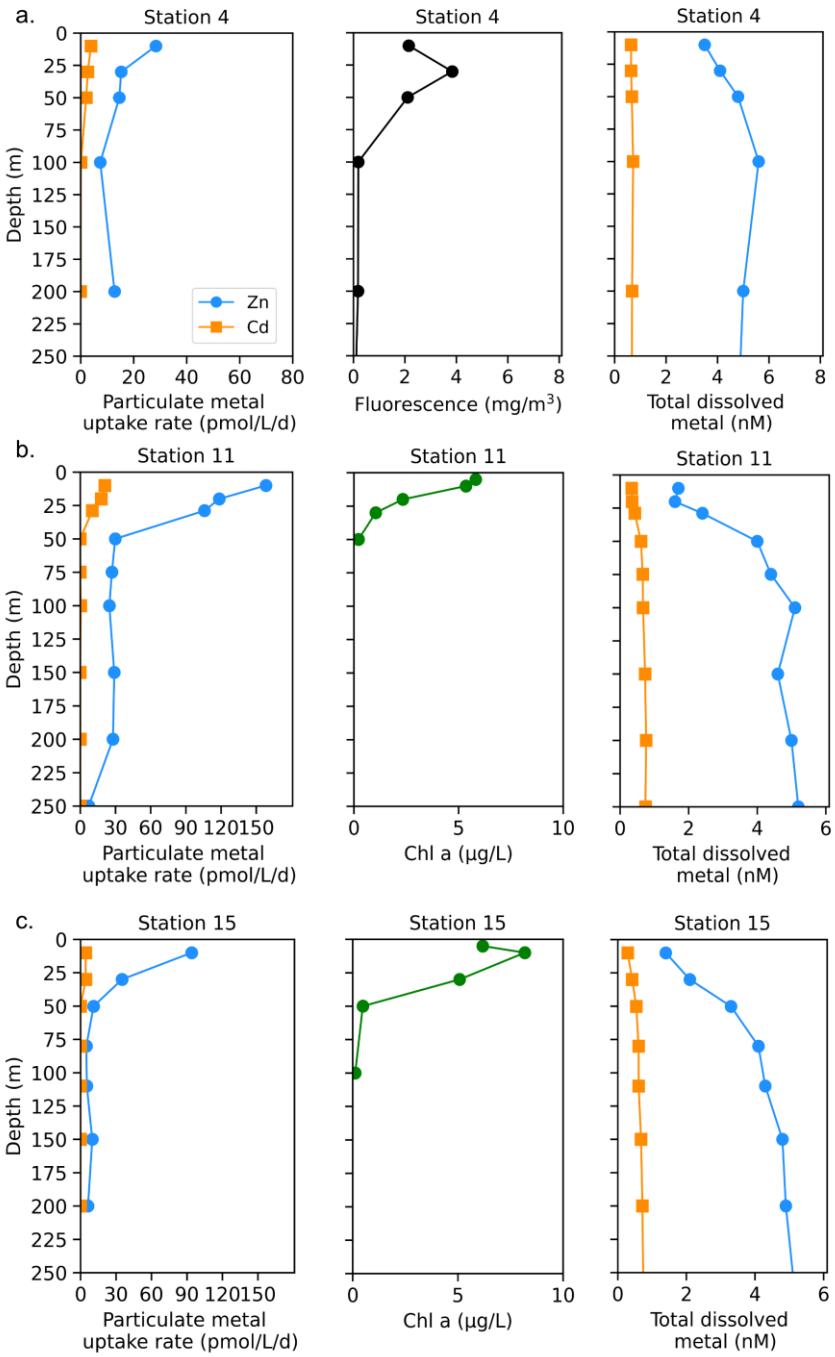

Figure 4. Depth profiles of total Zn and Cd uptake rates, total chlorophyll fluorescence (or chlorophyll *a*) and total dissolved metal measured in the upper 250 m at (a) station 4, (b) station 11, and (c) station 15 sampled along the Amundsen Sea shelf. Total chlorophyll (Chl) fluorescence is reported for stations where chlorophyll *a* (Chl a) data was not measured.

3.2 Ross Sea

We next investigated the dissolved Zn and Cd demand of the natural phytoplankton community at stations sampled over the Ross Sea shelf. Data collected from this group is presented over time, in order of sampling date (Fig. 5).

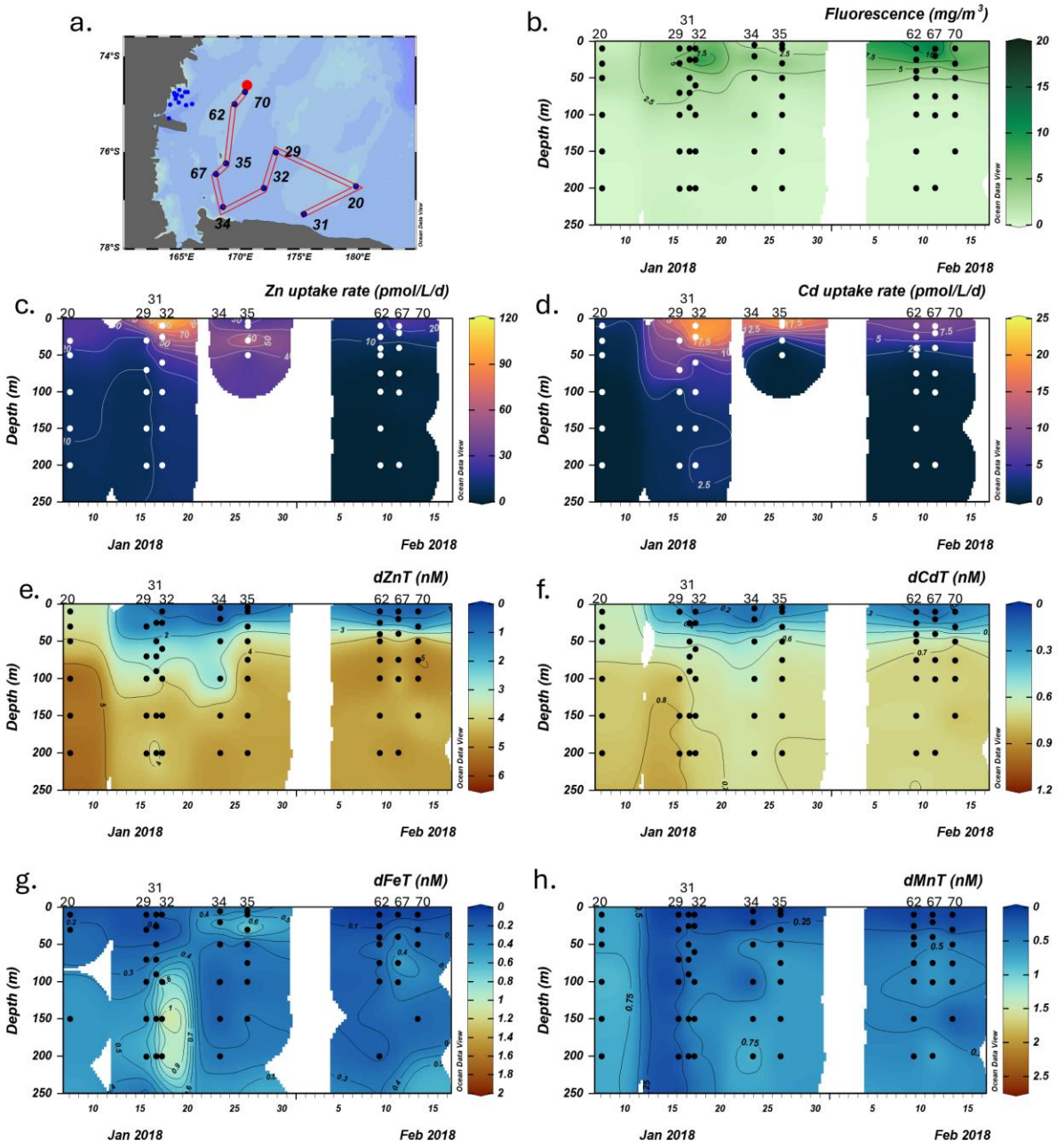

Figure 5. Total fluorescence and trace metal concentrations measured at Ross Sea stations shown over a latitudinal transect. (a) Map showing station locations, (b) total chlorophyll (Chl) fluorescence**,** (c) total Zn uptake rates, (d) total Cd uptake rates, (e) total dissolved Zn, (f) total dissolved Cd, (g) total dissolved Fe, and (h) total dissolved Mn measured in the upper 250 m

418 represented in color scale. Uptake experiments were not performed at stations 31, 34, and 70.
419 Metal concentrations measured to 800 m depth are shown in Figure S4. dZnT, total dissolved Zn;
420 dCdT, total dissolved Cd; dFeT, total dissolved Fe; dMnT, total dissolved Mn.
421

422 We note that unlike the Amundsen Sea sector, the stations sampled in this group did not
423 follow a linear cruise track, thus we cannot make inferences regarding latitudinal or longitudinal
424 changes. Surface Chl fluorescence was highest at stations 32 and 67 with maximum values of
425 15.8 and 14.6 mg m^{-3} at 25 m and 10 m, respectively (Fig. 5b). With the exception of station 20,
426 dZn and dCd demonstrated high levels of surface depletion within the upper 25 m (Fig. 5e,f)
427 with average concentrations of 0.63 ± 0.13 nM and 0.19 ± 0.09 nM respectively at ≤ 10 m.
428 Compared to 100 m values (i.e., below the MLD), concentrations at 25 m were equivalent to
429 87%, 34%, 85%, 85%, 77%, and 88% decreases in dZn and 83%, 19%, 84%, 67%, 64%, and
430 75% decreases in dCd at stations 32, 20, 67, 35, 29, and 62, respectively. Measured dMn
431 concentrations were also highly depleted within the upper 250 m at all Ross Sea stations
432 (average 10 m dMn = 0.18 ± 0.26 nM; Fig. 5h). While dFe was depleted within the upper 10 m at
433 all stations (average dFe concentration at 10 m = 0.12 ± 0.12 nM), concentrations exceeding 1
434 nM were observed below 100 m at station 32 (Fig. 5g) and extended down to 650 m (Fig. S4c),
435 implying a sedimentary source. The largest Zn uptake rate measured among all stations in this
436 group (115 pmol L^{-1} d^{-1}) was observed at station 32, 10 m (Fig. 6c). As observed in the
437 Amundsen Sea, ρZn, ρCd and total Chl a or Chl fluorescence profiles exhibited surface maxima
438 and became depleted with depth and were again mirrored by nutrient-like dZn and dCd depth
439 profiles (Fig. 6), indicative of uptake of these metals into the particulate phase in surface waters.

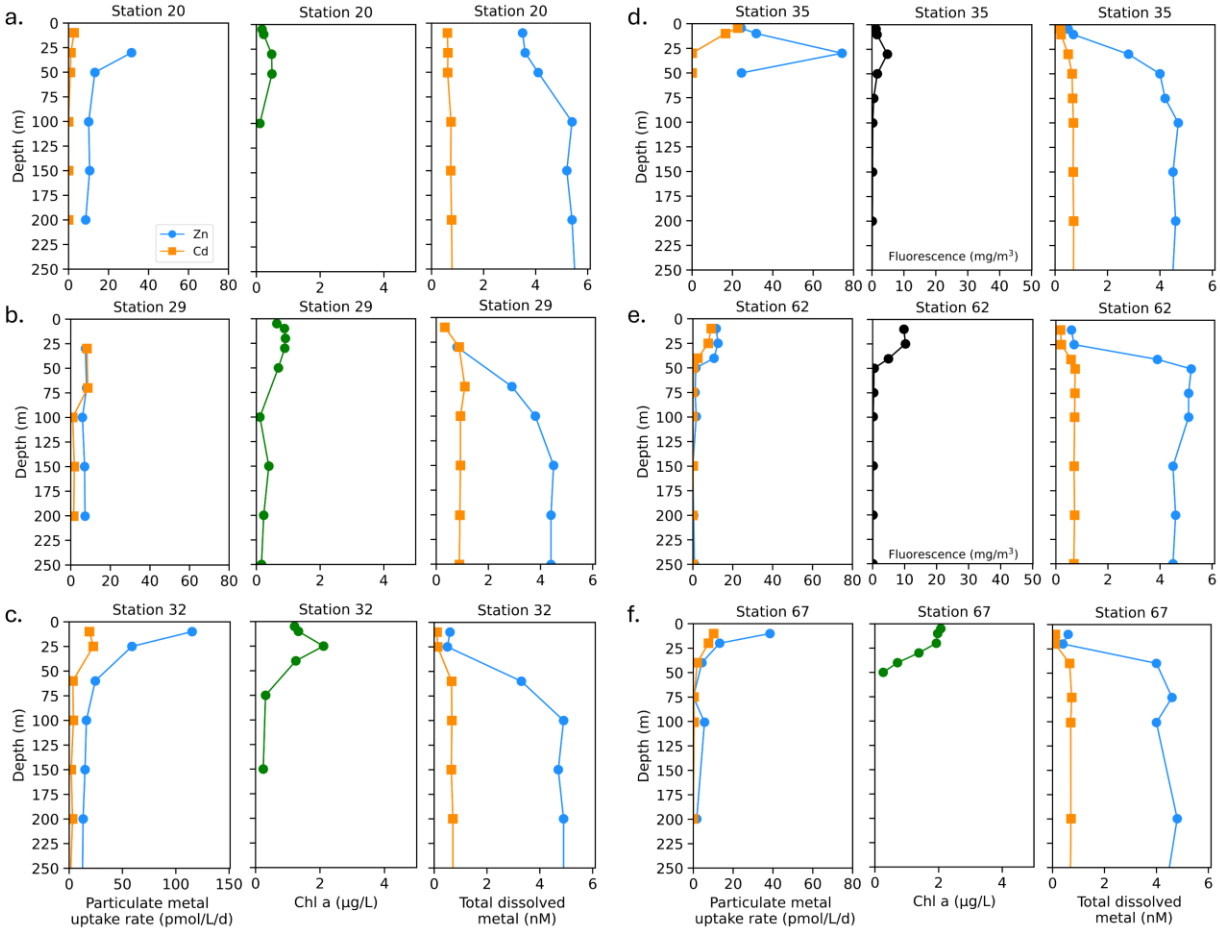

Figure 6. Depth profiles of total Zn and Cd uptake rates, total chlorophyll fluorescence (or, where available, chlorophyll a), and total dissolved metal ($dMetal_T$) measured in the upper 250 m at (a) station 20, (b) station 29, (c) station 32, (d) station 35, (e) station 62, and (f) station 67 sampled along the Ross Sea shelf. Total chlorophyll (Chl) fluorescence is reported for stations where chlorophyll a (Chl a) data was not measured.

3.3 Terra Nova Bay

Zinc and Cd uptake rate data collected from stations sampled in Terra Nova Bay (TNB) were visualized over time due to repeated sampling within a small geographic region and similar timeframe (Fig. 7a). This allowed for an analysis of how dissolved metal concentrations and metal uptake rates changed throughout January-February 2018 within the same spatial area.

Station data is presented in order of sampling date, from the earliest (station 22, sampled in early January) to the latest (station 79, sampled in late February).

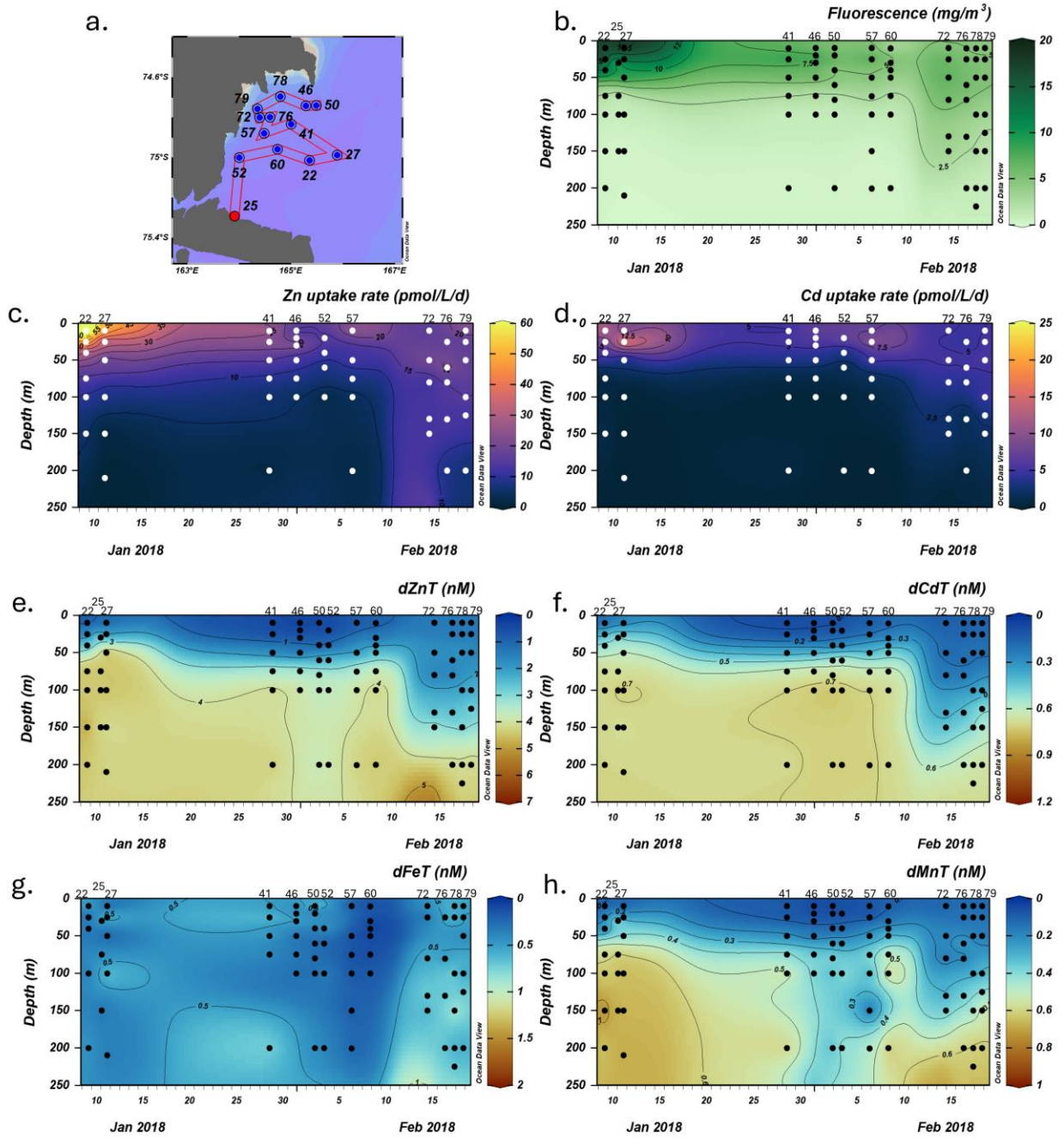

Figure 7. Total fluorescence and trace metal concentrations measured at Terra Nova Bay (TNB) stations shown over time. (a) Map showing station locations, (b) total chlorophyll (Chl) fluorescence, (c) total Zn uptake rates, (d) total Cd uptake rates, (e) total dissolved Zn, (f) total dissolved Cd, (g) total dissolved Fe, and (h) total dissolved Mn measured in the upper 250 m represented in color scale. Uptake experiments were not performed at stations 70 and 34. Metal

concentrations measured to 600 m depth are shown in Figure S5. dZnT, total dissolved Zn; dCdT, total dissolved Cd; dFeT, total dissolved Fe; dMnT, total dissolved Mn.

Surface Chl fluorescence was highest in early January (~18 mg m^{-3}) and waned into February (Fig. 7b), similar to observed trends in Zn and Cd uptake rates (Fig. 7 c,d). Of all TNB stations, stations 22 and 27, sampled in January, had the highest maximum Zn uptake rates of 89.9 pmol L^{-1} d^{-1} and 46.0 pmol L^{-1} d^{-1}, respectively, at 10 m (Fig. 8a,b). Cd uptake rates were also highest at these stations with values of 13.4 pmol L^{-1} d^{-1} and 20.1 pmol L^{-1} d^{-1} (Fig. 8a,b). At the final station (station 79, sampled in late February) maximum uptake rates of both metals had sharply decreased to 24.7 pmol Zn L^{-1} d^{-1} and 5.0 pmol Cd L^{-1} d^{-1} (Fig. 8i). Overall, maximum uptake rates of both metals decreased over time within TNB (Fig. 7c,d), consistent with the decrease in total Chl fluorescence (Fig. 7b) likely due to the aging and decline of the phytoplankton bloom.

Surface depletion of dZn, dCd, and dMn was observed at all stations with average dissolved concentrations of 0.82 ± 0.47 nM Zn, 0.13 ± 0.06 nM Cd, and 0.08 ± 0.04 nM Mn at 10 m depth (Fig. 7e,f,h). Notably, increased surface concentrations of dZn, dCd, and dMn were apparent at the late stations 72, 76, 78 and 79, with dZn ~2 nM, dCd ~300 pM, and dMn ~0.2 nM (Fig. 7e,f,h; Fig. S5). Dissolved macronutrient (phosphate, nitrate and nitrite, and silicate) concentrations also followed this trend, with increased surface concentrations at the late stations (Fig. S6). As with the Amundsen and Ross Sea station groups, Zn and Cd uptake rates within TNB tended to be highest at the surface ≤ 50 m as also observed in total Chl fluorescence trends and mirrored the decrease in total dissolved Zn and Cd (Fig. 8). Unlike the Amundsen and Ross Sea stations, where Cd uptake consistently became negligible (~0 pM L^{-1} d^{-1}) by 100 m (Fig. 4; Fig. 6), measurable Cd uptake persisted in TNB to 150 m at stations 72 and 79 (Fig. 8g,i).

Measurable Zn uptake rates were also captured at deeper depths at these late TNB stations (Fig. 8g,h,i).

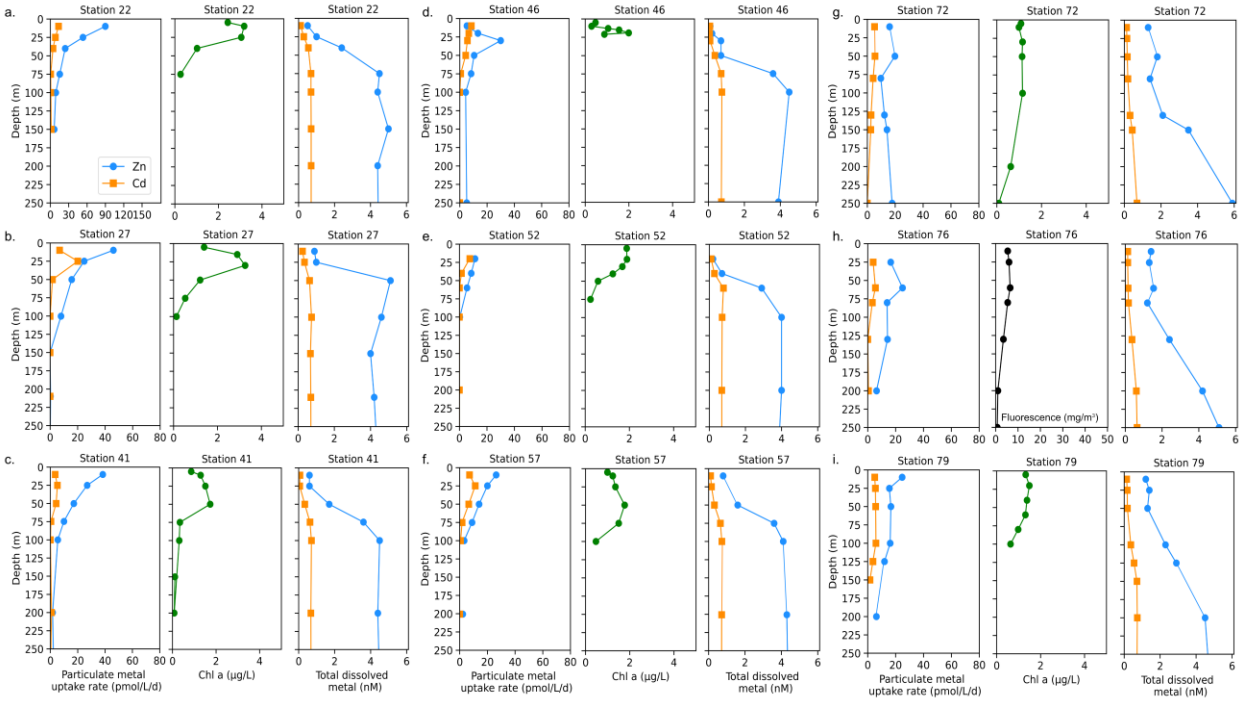

Figure 8. Depth profiles of total Zn and Cd uptake rates, total chlorophyll fluorescence (or, where available, chlorophyll a), and total dissolved metal (dMetalT) measured in the upper 250 m at (a) station 22, (b) station 27, (c) station 41, (d) station 45, (e) station 52, (f) station 57, (g) station 72, (h) station 76, and (i) station 79 within Terra Nova Bay. Total chlorophyll (Chl) fluorescence is reported for stations where chlorophyll a (Chl a) data was not measured.

The increased surface concentrations of dZn and dCd and macronutrients, as well as the persistence of measurable uptake rates at deeper depths, at these late TNB stations may be attributed to the deepening of the mixed layer (Fig. S7). Vertical mixing was evidenced by more uniform potential densities, temperatures, dissolved oxygen (O_2) concentrations, salinity, and beam transmission measurements at the late TNB stations within the upper 200 m (Fig. S7). Higher (>0.5 nM) dFe concentrations were also observed below 100 m at these late stations (Fig. 7g) and increased with depth (>2 nM), as did dZn and dMn concentrations, possibly due to sedimentary inputs (Giordano et al., 1999) (Fig. S5). At these late stations (Station 76, 78, 79)

mixing replenished surface concentrations of both macronutrients (Fig. S6) and dZn (Fig. S5a), but dZn was replenished to a lower extent. For example, comparing 50 m "replenished" surface values of P, N+N, and Si to deepwater (200 m) values at Station 79, percent changes from deep to surface values were -0.35% for P, -0.30% for N+N, and -0.26% for Si (where a percent change of 0 would indicate complete replenishment; i.e, if nutrient values at 200 m and at 50 m were equal). In contrast, the percent change from deep (200m) to surface (50m) dZn at Stn79 was lower, -0.71%. Hence, dZn was apparently replenished to a lesser extent compared to macronutrients, which may reflect a sustained high demand for Zn generating a dearth of this micronutrient despite macronutrient replenishment.

3.4 Overview of Zn and Cd uptake at 18 stations

We next summarize the maximum Zn and Cd uptake rates observed at each station (all of which were observed at ≤ 10 m depth; Fig. 9a,b) with uptake rates normalized to Chl a (µg/L) as a proxy for biomass (Fig. 9c,d).

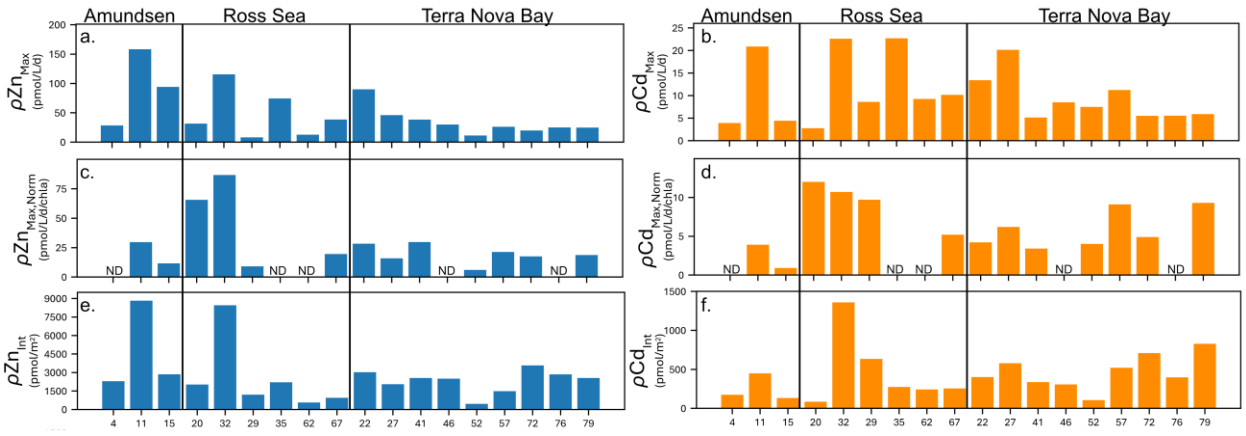

Figure 9. Unnormalized (a) maximum Zn uptake rates (ρZn_{Max}) and (b) maximum Cd uptake rates (ρCd_{Max}) at each station grouped by area (Amundsen Sea, Ross Sea, Terra Nova Bay). (c) ρZn_{Max} and (d) ρCd_{Max} normalized to chlorophyll a (µg L^{-1}) measured at each station. (e) Depth integrated (10 m-250 m) ρZn and ρCd values at each station. ND, no data (chlorophyll a not measured).

Overall, high (>25 pmol L^{-1} d^{-1} Chl a (ug/L) $^{-1}$) Chl a-normalized Zn uptake rates were measured at station 11 in the Amundsen Sea and at stations 20 and 32 in the Ross Sea (Fig. 9c). The highest Chl a-normalized Cd uptake rates among all 18 stations were also measured at stations 20 and 32 (Fig. 9d). Across TNB, Chl a-normalized maximum Zn and Cd uptake ranged from 6.0 – 28.3 pmol L^{-1} d^{-1} Chl a^{-1} for Zn, and 3.4 – 9.3 pmol L^{-1} d^{-1} Chl a^{-1} for Cd; Fig. 9c,d). Integrated (10 m-250 m) uptake rate values were highest for Zn at stations 11 and 32, and highest for Cd at station 32 (Fig. 9e,f). Increases in integrated Cd and Zn uptake at the late stations 72, 76 and 79 reflected the deeper depths to which uptake rates of these metals remained measurable, likely reflecting deepened mixed layers (Fig. S7) and/or sinking of the phytoplankton community, as seen in the fluorescence data to beyond 150m depth (Fig. 7b). The presence of Chl a (Fig. 8g,i) implies these deep phytoplankton communities may have been alive, if not actively photosynthesizing. We previously identified ZCRP-B, a membrane-associated protein involved in high-affinity Zn transport (Kellogg et al., 2022). These proteins have a single transmembrane domain, implying function as a membrane-tethered ligand to assist in the acquisition of Zn from seawater in cooperation with adjacent zinc transporters (ZIP transporters). Hence ZCRP-B could be a potential site of Zn binding and 'uptake', as our uptake rate measurements do not discern between extracellular and intracellular Zn, even if the phytoplankton are inactive due to a lack of photosynthetic energy at these depths.

Notably, maximum Cd uptake rates measured in the present study were 3.4, 3.7, and 3.3 times higher in the Amundsen Sea, Ross Sea, and Terra Nova Bay, respectively, compared to the maximum Cd uptake rate of 6.1 pmol L^{-1} d^{-1} measured previously within the Costa Rica Dome using identical methods (Cox et al., 2014), demonstrating the influence of high productivity and the native community on the flux of dCd into the particulate phase.

4 Discussion

4.1 Use of metal uptake rates to determine depletion timeframes

The measurement of total dissolved metal concentrations over large latitudinal or longitudinal areas allows for the characterization of metal inventories, though these are snapshots of inventories observed at specific times. The measurement of metal uptake rates allows us to gain new insight into how these inventories came to be and the timeframes over which they are consumed and replenished. Due to the resetting of surface dissolved metal concentrations to those of deepwater values during austral winter with deep winter mixing, the Ross Sea of the Southern Ocean is particularly applicable to this type of timeframe study (Sedwick and DiTullio 1997; Sedwick et al. 2011).

Using the Zn uptake rates measured in this study, we can estimate the time required for the high levels of primary production observed in the Southern Ocean to draw down surface dZn from high (deep water) winter concentrations to the surface concentrations observed during austral summer 2017. The Southern Ocean growing season typically spans October-March, with primary productivity peaking November-January and the area of open (ice-free) water over the Ross Sea shelf linearly increasing from November-mid January (Sedwick et al., 2011). Vertical profiles of nutrients and micronutrients in coastal Antarctic ecosystems such as the Ross Sea are reset and become uniform with depth during the winter months due to whole water column mixing and an absence of photosynthetic activity during the dark winter under the sea ice (Noble et al., 2013). As a result, the drawdown of nutrients in the upper water column observed during the spring and summer seasons is the result of less than one year's biological influence. For this simple calculation, we ignore the upward flux of Zn (upwelling = 0) and assume a high export ratio of 0.8 due to bloom productivity being dominated by diatoms and *Phaeocystis antarctica*,

both of which sink rapidly and thus contribute substantially to carbon export flux (Asper and Smith 1999; DiTullio et al. 2000). The depletion of dZn from a surface box was therefore estimated as:

$$\left(\frac{dZn}{dt}\right)_{surface\ box} = -\rho Zn\ + (Rf * \rho Zn) + upwelling$$

Where Rf is the remineralization factor equal to 1 - export ratio.

Taking station 11, for which the highest Zn uptake rate was observed, as an extreme case: with a maximum Zn uptake rate of 158 pmol L^{-1} d^{-1}, it would take only 25 days to deplete a surface winter concentration of 4.8 nM (that is, the average deepwater (< 200 m) dZn concentration for all stations measured in this study) down to the observed surface concentration of 1.7 nM at station 11 (Fig. 4b), assuming a constant uptake rate and no additional inputs of dissolved Zn (Fig. 10).

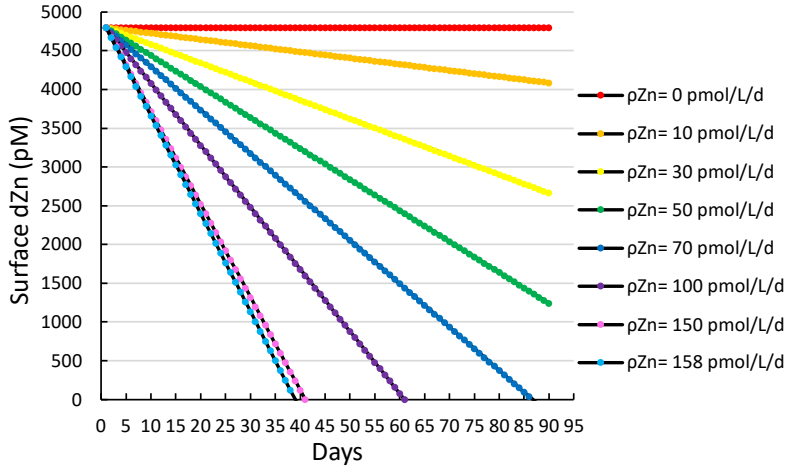

Figure 10. A simple model estimating the time (in days) required to deplete the estimated average winter surface concentration of dZn (4.8 nM) over a range of various Zn uptake rates (ρZn). 158 pmol/L/d was the maximum Zn uptake rate observed in this study (station 11, 10 m).

Given that dZn surface depletion to sub-nanomolar levels was observed throughout much of the CICLOPS expedition, prolonged high levels of Zn uptake and export that overwhelm

587 replenishment by vertical mixing and/or remineralization are likely key to giving rise to the
588 observed extent of seasonal surface dZn depletion. These calculations were conducted as a proof-
589 of-concept to determine if uptake rates were sufficient to draw down the otherwise abundant dZn
590 inventory on seasonal timescales. An important caveat to this calculation is that the regulation
591 and production of Zn sensors that modulate Zn uptake, export, and storage will naturally
592 fluctuate in response to changing dZn and therefore cannot be assumed as a constant. Future
593 studies could conduct mesoscale modeling of the region, including eddy diffusion and advection.
594 Notably, any dZn upwelling flux into the euphotic zone would require even higher Zn uptake
595 rates to create the seasonal surface Zn depletion we observed on this expedition.
596
597 **4.2 Influences on Zn and Cd uptake**
598 We next consider the factors driving the magnitude of ρZn and ρCd. As noted above, ρZn
599 and ρCd were positively correlated with total Chl fluorescence or Chl a at every station (Fig. 4;
600 Fig. 6; Fig. 8), demonstrating the influence of total autotrophic biomass on uptake rates. A
601 Pearson correlation analysis comparing the abundance of individual algal pigments to ρZn and
602 ρCd throughout the water column for all stations revealed significant, positive correlations
603 (Pearson correlation coefficient > 0.50, $p \leq 1.2e\text{-}4$) between ρZn and Chl *a*, Chl *b*, and Chl c1, c2
604 and c3. Pearson correlation coefficients are normally symbolized as rho (ρ), but to avoid
605 confusion with our uptake rate symbol (ρ), and with p-values (p), they are herein referred to as
606 'PCC' values. The correlation between ρZn and Chl *b* was strongest (PCC= 0.77, p = 3.8e-10) of
607 any pigment (Fig. 11e).

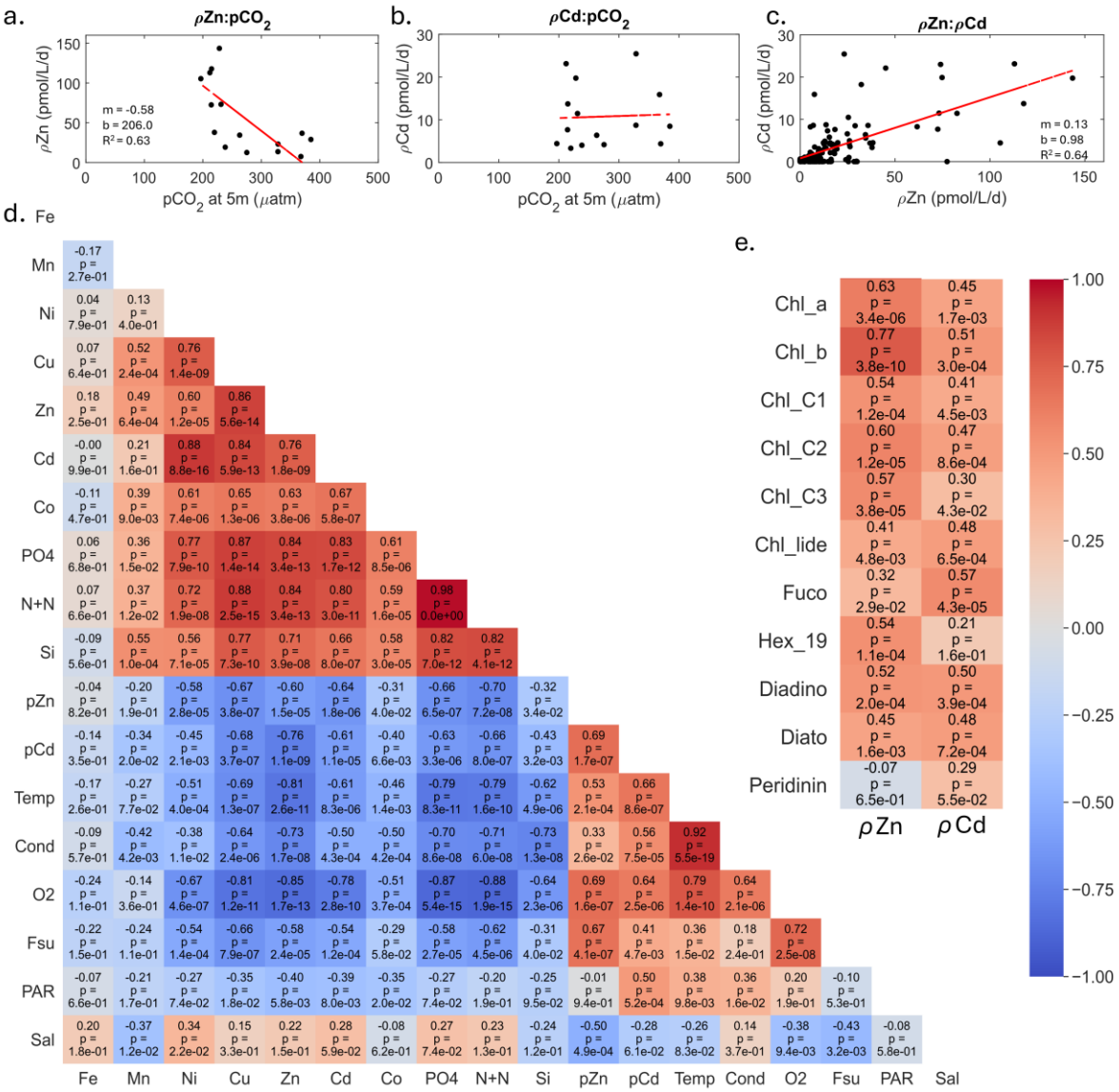

Figure 11. Relationships comparing seawater CO_2 partial pressure (pCO_2) at 5 m depth to (a) Zn uptake rates (ρZn; n=15, R^2 = 0.63) and (b) Cd uptake rates (ρCd; n=15) measured at surface (≤10 m) depths. (c) Relationship between ρZn and ρCd for all depths (n=121, R^2 = 0.64). (d) Visual representation of the correlation matrix comparing all water column parameters measured with depth with warm and cool colors indicative of positive and inverse correlations, respectively. Pearson correlation coefficients and p values are shown. (e) Representation of the correlation matrix comparing ρZn and ρCd to various phytoplankton pigments. Fe, Mn, Ni, Cu, Zn, Cd, and Co labels correspond to total dissolved metal concentrations. PO4, N+N, and Si correspond to total dissolved concentrations of phosphate, the sum of nitrate+nitrite, and silicate. Temp, temperature; cond, conductivity; O_2, dissolved oxygen; Fsu, total fluorescence; PAR, photosynthetically active radiation; Sal, salinity. Chl_a, chlorophyll *a*; Chl_b, chlorophyll *b*; Chl_c1, chlorophyll c1; Chl_c2, chlorophyll c2; Chl_c3, chlorophyll c3; chl_lide, chlorophyllide; Fuco, fucoxanthin; Hex_19, 19'-hexanoyloxyfucoxanthin; Diadino, diadinoxanthin; Diato, diatoxanthin.

In bottle incubation experiments conducted at station 27, the addition of Zn alone resulted in the positive growth response of Chl *b*-containing algae (small green algae such as prasinophytes; (Kell et al., 2023)), corroborating this finding. ρCd also positively correlated with these Chl pigments but with slightly lower correlation Pearson correlation coefficients (PCC = 0.3-0.51; $p \leq .043$). Fucoxanthin (fuco) concentrations were more highly correlated with ρCd (PCC = 0.57, p = 4.3e-5) than with ρZn (PCC = 0.32, p =2.9e-2), while the opposite was observed for 19'-Hex (19'-hexanoyloxyfucoxanthin; PCC = 0.54, p = 1.1e-4 for Zn; not significant for Cd) (Fig. 11e). Fuco and 19'-Hex are used as taxonomic indicators of diatoms and *Phaeocystis*, respectively, in the Ross Sea (DiTullio et al., 2003, 2007; DiTullio and Smith, 1995; Wright et al., 2010). The higher correlation coefficient between ρZn and *Phaeocystis* abundance (as indicated by 19'-Hex) implies that Zn uptake was driven largely by *Phaeocystis*. This finding is consistent with the detection of *Phaeocystis* ZCRP-A, a protein characterized as an algal Zn^{2+} metallochaperone (Kellogg et al., 2022), in metaproteomic data collected from both the incubation experiment and throughout the water column at station 27 (Kell et al., 2023). The positive correlation between ρCd and the abundance of diatoms (as indicated by fuco) is consistent with the diatomic utilization of Cd as a nutrient within CDCA metalloenzymes, as *cdca* genes have, to date, been found exclusively in diatom species (Park et al., 2007, 2008). While it is likely that both *Phaeocystis* and diatoms contributed to the Cd and Zn uptake rates measured here, it is currently unknown if *Phaeocystis* can utilize Cd as a nutrient. Overall, any potential growth benefit conferred by our Cd spike additions may only have been applicable to diatoms that 1) possessed the *cdca* gene and 2) faced selection pressure to utilize Cd as a cofactor in CDCA due to low seawater pCO_2 (as documented on this expedition) creating enhanced demand for dZn. The presence of Cd-utilizing diatoms in the water column at station

27 was demonstrated by the detection of CDCA transcripts with closest taxonomic matches to the diatom genera *Chaetoceros* and *Corethron* (Kell et al., 2023). Station 27 also exhibited high surface Chl fluorescence (19.3 mg m^{-3} at 10 m), low pCO_2 (221 μatm at 5 m), and high maximum Zn and Cd uptake rates (46 and 20 pmol L^{-1} d^{-1}, respectively), demonstrating a high algal demand for Zn that likely created pressure for Cd uptake.

We next consider the effect of the depleted seawater pCO_2 levels induced by the high biomass conditions observed on this expedition. Previously, a strong correlation between dissolved $\delta^{114}Cd$ and dissolved CO_2 was documented in the Atlantic Sector of the Southern Ocean (de Baar et al., 2017), suggesting significant Cd isotope fractionation due to biological uptake into the particulate phase. A relationship between total surface Cd uptake rates at 10 m and surface pCO_2 (underway, measured at 5 m) was not observed in the present study (Fig. 11b). The present study includes measurements of total Cd uptake (that is, the sum of all Cd isotopes) using an added Cd isotope tracer, and hence did not explore natural isotope fractionation effects. However, we did observe a significant negative linear relationship between total Zn uptake rates and seawater pCO_2 ($m = -0.58$; $R^2 = 0.63$; Fig. 11a) consistent with an increased demand for Zn^{2+} to power the carbon concentrating mechanism of photosynthetic algae under lower CO_2 availability. ρZn and ρCd furthermore shared a significant positive linear relationship with each other ($m = 0.13$; $R^2 = 0.64$; Fig. 11c) (as was also reflected in the Pearson correlation test; PCC = 0.69, p = 1.7e-7, Fig. 11d) implying that as demand for Zn increased, demand for Cd also increased, consistent with laboratory studies showing their co-transport in marine algae (Sunda and Huntsman, 2000). We also note that ρCd:ρZn uptake ratios were higher (> 0.4) at the surface where total dissolved dCd:dZn ratios were comparatively higher (> 0.3) (Fig. S8a,b). The strong positive linear relationship shared between these ratios ($R^2 = 0.82$; Fig. S8c) further suggests that

dZn levels were depleted enough to induce increased Cd uptake rates, and is consistent with their known biochemical substitution within marine algae.

Algal Cd uptake rates are known to be inversely related to both Mn^{2+} and Zn^{2+} concentrations in culture (Lee et al., 1995; Sunda and Huntsman, 1996), which is thought to reflect the uptake of Cd by two separate inducible transport systems. Cd is taken up competitively by the high-affinity Zn uptake system under low Zn^{2+} conditions, as demonstrated above, while Cd, Zn, and Mn share the same low-affinity Mn uptake system under high Zn^{2+} conditions (Lee et al., 1995; Sunda and Huntsman, 1998b, a, 2000; Xu et al., 2007). With the exception of the Amundsen Sea stations, dMn was consistently observed at concentrations of only 0.1-0.5 nM within the upper 50 m (Fig. 3h; Fig. 5h; Fig. 7h). Low surface dMn concentrations within the Southern Ocean have been documented previously and were attributed to a combination of biological uptake at the surface causing depletion and low resupply due to few external sources (Latour et al., 2021). While ρCd was negatively correlated with dMn (PCC = -0.34, p = 0.02) considering all stations and all depths, ρCd was more strongly negatively correlated with dZn (PCC = -0.76, p = 1.1e-9), which was the strongest negative correlation comparing all measured parameters to ρCd (Fig. 11d). This finding is consistent with decreased dCd uptake where dZn availability is sufficient. Overall, these results are consistent with biology (total biomass) and pCO_2 acting as primary influences on ρZn, with increases in ρZn leading to increases in ρCd through the upregulation of a shared transport system.

4.3 Effects on dCo cycling

In addition to Cd, the intense Zn demand captured by these uptake rates also appears to have shifted the demand for the trace metal micronutrient cobalt (Co) (Chmiel et al., 2023). Due to their similar charge and atomic radii, Zn^{2+}, Co^{2+} and Cd^{2+} cations often share the same

transporter uptake systems. An organism's ability to utilize these metals as metabolic cofactors is influenced by their environment and the affinity of the uptake ligands for each metal cation (Irving and Williams, 1953; Sunda and Huntsman, 1992). When dZn availability is low, more dCd and dCo are able to bind transport ligands. Therefore, dZn concentrations and cycling can influence the cycling of dCd and dCo, particularly in low dZn environments as documented for dCd in the present study. The influence of dZn cycling on dCo distributions in this region was also documented during this expedition, with evidence for high rates of biological Co uptake in the Ross Sea driven by dZn (and vitamin B_{12}) scarcity (Chmiel et al., 2023). The high Zn uptake rates measured in this study therefore also reveal dynamic changes in the cycling of Cd and Co as a consequence of high Zn demand.

4.4 dZn and dCd relationships with macronutrients

The growth of phytoplankton and bacteria in the shallow euphotic zone results in the removal of bioactive trace metals and macronutrients from the dissolved phase into the particulate phase, resulting in dissolved metal:macronutrient relationships that reflect their collective stoichiometry (Horner et al., 2021). Positive linear slopes result generally indicate the co-cycling of the metal and the macronutrient via uptake and remineralization, though slope values can vary widely by basin as they are a function of the metal:macronutrient uptake and remineralization stoichiometry of the native community and overall nutrient availability. Two-way linear regressions (see Methods) were used to investigate the relationships between dZn and dissolved silicate (dSi), dZn and dissolved phosphate (dP), and dCd and dP for the Amundsen Sea, Ross Sea, and TNB station groups (Fig. 12).

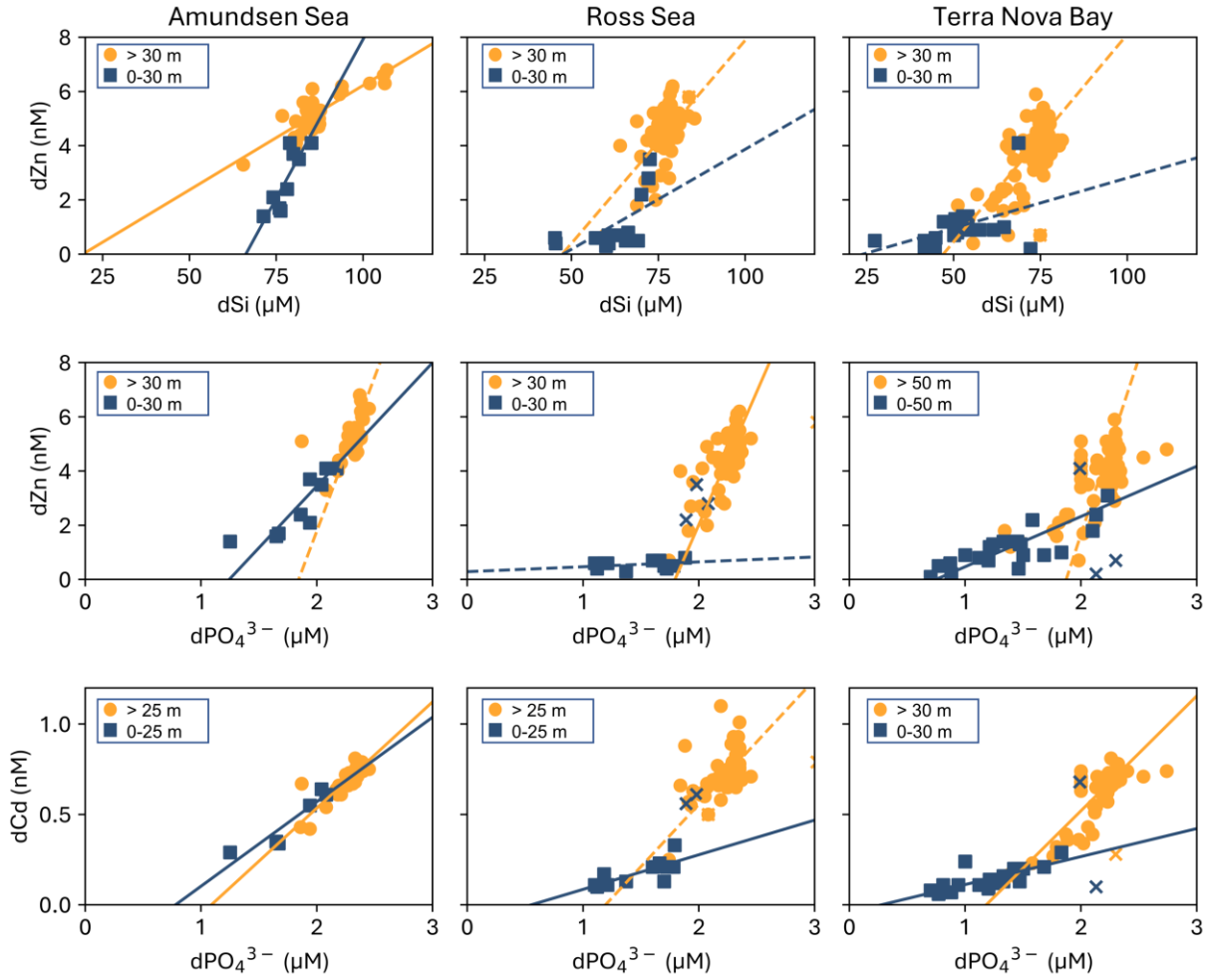

Figure 12. Relationships between (top row) total dissolved Zn and silicate (dSi) (top row), total dissolved Zn and phosphate (dPO_4^{3-}) (middle row), and total dissolved Cd and dPO_4^{3-} (bottom row) for surface (blue squares) and deep ocean (orange circles) arranged by station group (Amundsen Sea, Ross Sea, and Terra Nova Bay). Depth thresholds were manually chosen to optimize the linear fit of the surface and deep ocean trends. Regressions with an $R^2 \geq 0.50$ are shown as a solid line, and those with an $R^2 < 0.50$ are shown as a dotted line. See Table S4 for stoichiometric parameters and values. Regression outliers are marked with an 'x'. Data originally plotted in Chmiel et al. 2023 and reprised here for ease of comparison with dZn:Si data.

The dZn:dP and dCd:dP relationships from this expedition were originally presented in Chmiel et al. 2023 for comparison to dCo:dP, while they are included in the present study for ease of comparison with dZn:dSi relationships presented for the first time. For these analyses, the depth threshold that separates the surface and deep ocean was manually defined in order to

optimize the linear fit of the surface versus deep trends— this threshold depth can be thought of as an inflection point that represents the largest change in trace metal concentration with respect to dP or dSi concentration (Chmiel et al., 2023).

The near-linear global dZn:dSi relationship (Bruland et al., 1978; Middag et al., 2019; Vance et al., 2017) has been posited to arise, in part, from faster drawdown of Zn and Si relative to dPO_4^{3-} into Southern Ocean diatoms that leaves surface waters Zn and Si depleted (Vance et al., 2017). We observed distinct differences in dissolved dZn:dSi ecological stoichiometries comparing Amundsen Sea, Ross Sea and Terra Nova Bay station groups (Fig. 12; Table S4). A positive linear dZn:dSi relationship with a steep ($m = 0.23 \pm 0.05$; Table S4) slope observed in the upper ocean of the Amundsen Sea contrasted starkly with the shallow slopes observed in the upper ocean of the Ross Sea and Terra Nova Bay. A bloom of non-silicifying *Phaeocystis antarctica* was present during our passage through the Amundsen Sea, consistent with abundant silicic acid yet rapid drawdown of Zn, which is known to be used by this organism (Saito and Goepfert, 2008). In contrast, the shallow slopes in the Ross Sea and Terra Nova Bay resulted from the persistence of dSi concentrations ≥ 30 μM in the upper 30 m,while dZn was reduced to sub-nanomolar concentrations (average dZn = 0.87 ± 0.42 nM in TNB at 10 m depth, n= 11), highlighting the intense drawdown of dZn by biota in this region to meet a high metabolic dZn demand.

Similar trends were observed for dZn:dP and dCd:P, which exhibited shallow slopes within the upper ocean of the Ross Sea and Terra Nova Bay. Southern Ocean diatoms are known to have Zn:P uptake ratios that are up to an order of magnitude greater than the average for oceanic phytoplankton (Sieber et al., 2020; Twining and Baines, 2013; Vance et al., 2017). The increased presence of diatoms (as indicated by higher fucoxanthin concentrations) at the late

753 stations within Terra Nova Bay therefore likely exacerbated the surface decoupling of dZn and
754 dP due to their high dZn demand. The maximum uptake rates of 158, 115, and 89 pmol Zn L^{-1} d^{-1}
755 measured in this study for the Amundsen Sea, Ross Sea, and Terra Nova Bay groups,
756 respectively, contextualize the high Zn uptake rates hypothesized to contribute to the high dZn:
757 dP uptake ratios observed in Southern Ocean diatoms. These rates are indicative of total potential
758 biological uptake, likely influenced by a depleted labile Zn pool and residual of complexed Zn,
759 that then results in low dZn:dP ratios in shallow waters.

760 Like dZn and dSi, dCd and dP concentrations are known to share strong correlations in
761 both deep and surface seawater (de Baar et al., 1994; Boyle, 1988; Boyle et al., 1976), with the
762 vertical distribution of Cd controlled by phytoplankton uptake in surface waters and sinking of
763 particulate organic matter and subsequent remineralization at depth. Observations of enhanced
764 Cd uptake within the Fe-limited Southern Ocean (Cullen, 2006) are consistent with observations
765 of increased Cd uptake by marine algal species under Fe limitation in both the field (Baars et al.,
766 2014; Cullen et al., 2003; Cullen and Sherrell, 2005) and in culture (Lane et al., 2009; Sunda and
767 Huntsman, 2000), thought to be due to the increased use of Cd in biochemical processes or
768 inadvertent uptake due to the upregulation of metal transporters (Cullen, 2006; Sunda and
769 Huntsman, 2000). In these coastal regions, dCd:dP had the same regional and depth trends as
770 dZn:dP, further demonstrating their close biogeochemical association.

771 **5 Conclusions**

772 We have quantified the movement of the trace metals Zn and Cd from the dissolved to
773 the particulate phase within the phytoplankton >3 μm size fraction collected in the Amundsen
774 Sea, Ross Sea, and Terra Nova Bay of the Southern Ocean during austral summer 2017-2018.
775 Our study adapts the stable Cd isotope tracer uptake method (Cox et al., 2014) to the

measurement of Zn uptake, and represents the first time series measurements of dZn and Zn uptake in a coastal environment during a bloom event. We have found that these high observed uptake rates were sufficient to draw down the otherwise abundant dZn inventory on seasonal timescales. Our analysis suggests that enhanced total biomass and low pCO_2 act as primary influences on ρZn, and that high ρZn results in dynamic changes in the cycling of both Cd and Co as a consequence of high Zn demand. Low dZn:Si slope values observed in the Ross Sea and Terra Nova Bay further highlighted the intense drawdown of dZn by biota to meet a high metabolic dZn demand. Overall, our study demonstrates that Zn demand is high and rapid enough to depress the inventory of Zn available to phytoplankton, suggesting that Zn has been overlooked as a dynamic limiting micronutrient in primary productivity modeling.

Data availability

CICLOPS (NBP18-01) CTD hydrography data (including pressure, temperature, total dissolved oxygen, conductivity, fluorescence, and beam transmission; https://www.bco-dmo.org/dataset-deployment/783917) in addition to total dissolved metal, Zn and Cd uptake rate, macronutrient, and pigment datasets are available through the NSF Biological and Chemical Oceanography Data Management Office (BCO-DMO) repository (https://www.bco-dmo.org/deployment/778919). Underway pCO_2 data collected during cruise NBP1801 is available through R2R, https://doi.org/10.7284/139318.

Author contributions

Conceptualization and analysis of the study was carried out by RMK and MAS. This work was supervised by MAS and GRD. Funding was acquired by MAS and GRD. RJC and DR contributed dCo data and discussion. DMM, MRM, NLS, IS, and RBD aided in sampling and data collection. TJH contributed to analysis and discussion. RMK and MAS wrote the manuscript with review and editing contributions from all co-authors.

Competing interests

The authors declare that they have no conflict of interest.

Acknowledgements

We thank the captain, crew, marine technicians, and science party of RVIB Nathaniel B. Palmer for their support and contributions to the success of the NBP18-01 cruise, Joe Jennings (OSU) for conducting macronutrient analyses, Lauren Lees for assistance with sampling, and Natalie Cohen for assistance in operation of the seaFAST and application of the isotope dilution technique.

Funding

National Science Foundation grant 2123055 (MAS)

National Science Foundation grant 2125063 (MAS)

National Science Foundation grant 1643684 (MAS)

National Science Foundation grant 1924554 (MAS)

National Science Foundation grant NSF-PLR 1643845 (RBD)

Simons Foundation (MAS)

National Science Foundation grant NSF-OPP 1644073 (GRD)

TJH acknowledges support from the Woods Hole Oceanographic Institution's *Ocean and Climate Innovation Accelerator* program.

References

Arrigo, K. R., van Dijken, G. L., and Bushinsky, S.: Primary production in the Southern Ocean, 1997–2006, Journal of Geophysical Research, 113, C08004, https://doi.org/10.1029/2007JC004551, 2008.

Arrigo, K. R., Lowry, K. E., and van Dijken, G. L.: Annual changes in sea ice and phytoplankton in polynyas of the Amundsen Sea, Antarctica, Deep Sea Research Part II: Topical Studies in Oceanography, 71–76, 5–15, https://doi.org/10.1016/j.dsr2.2012.03.006, 2012.

de Baar, H. J. W., Saager, P. M., Nolting, R. F., and van der Meer, J.: Cadmium versus phosphate in the world ocean, Marine Chemistry, https://doi.org/10.1016/0304-4203(94)90082-5, 1994.

de Baar, H. J. W., van Heuven, S. M. A. C., Abouchami, W., Xue, Z., Galer, S. J. G., Rehkämper, M., Middag, R., and van Ooijen, J.: Interactions of dissolved CO2 with cadmium isotopes in the Southern Ocean, Marine Chemistry, 195, 105–121, https://doi.org/10.1016/J.MARCHEM.2017.06.010, 2017.

Baars, O. and Croot, P. L.: The speciation of dissolved zinc in the Atlantic sector of the Southern Ocean, Deep Sea Research Part II: Topical Studies in Oceanography, 58, 2720–2732, https://doi.org/10.1016/j.dsr2.2011.02.003, 2011.

Baars, O., Abouchami, W., Galer, S. J. G., Boye, M., and Croot, P. L.: Dissolved cadmium in the Southern Ocean: Distribution, speciation, and relation to phosphate, Limnology and Oceanography, 59, 385–399, https://doi.org/10.4319/LO.2014.59.2.0385, 2014.

Bertrand, E. M., Saito, M. A., Rose, J. M., Riesselman, C. R., Lohan, M. C., Noble, A. E., Lee, P. A., and DiTullio, G. R.: Vitamin B 12 and iron colimitation of phytoplankton growth in the Ross Sea, Limnology and Oceanography, 52, 1079–1093, https://doi.org/10.4319/lo.2007.52.3.1079, 2007.

Biller, D. V. and Bruland, K. W.: Analysis of Mn, Fe, Co, Ni, Cu, Zn, Cd, and Pb in seawater using the Nobias-chelate PA1 resin and magnetic sector inductively coupled plasma mass spectrometry (ICP-MS), Marine Chemistry, https://doi.org/10.1016/j.marchem.2011.12.001, 2012.

Bishop, J. K. B. and Wood, T. J.: Year-round observations of carbon biomass and flux variability in the Southern Ocean, Global Biogeochemical Cycles, https://doi.org/10.1029/2008GB003206, 2009.

Bown, J., Laan, P., Ossebaar, S., Bakker, K., Rozema, P., and de Baar, H. J. W.: Bioactive trace metal time series during Austral summer in Ryder Bay, Western Antarctic Peninsula, Deep-Sea Research Part II: Topical Studies in Oceanography, https://doi.org/10.1016/j.dsr2.2016.07.004, 2017.

Boyle, E. A.: Cadmium: Chemical tracer of deepwater paleoceanography, Paleoceanography, https://doi.org/10.1029/PA003i004p00471, 1988.

Boyle, E. A., Sclater, F., and Edmond, J. M.: On the marine geochemistry of cadmium, Nature, https://doi.org/10.1038/263042a0, 1976.

Brand, L. E., Sunda, W. G., and Guillard, R. R. L.: Reduction of marine phytoplankton reproduction rates by copper and cadmium, Journal of Experimental Marine Biology and Ecology, https://doi.org/10.1016/0022-0981(86)90205-4, 1986.

Bruland, K. W., Knauer, G. A., and Martin, J. H.: Zinc in north-east Pacific water, Nature, 271, 741–743, https://doi.org/10.1038/271741a0, 1978.

862 Chmiel, R. J., Kell, R. M., Rao, D., Moran, D. M., DiTullio, G. R., and Saito, M. A.: Low cobalt
863 inventories in the Amundsen and Ross seas driven by high demand for labile cobalt uptake
864 among native phytoplankton communities, Biogeosciences, 20, 3997–4027,
865 https://doi.org/10.5194/bg-20-3997-2023, 2023.

866 Cox, A. D., Noble, A. E., and Saito, M. A.: Cadmium enriched stable isotope uptake and
867 addition experiments with natural phytoplankton assemblages in the Costa Rica Upwelling
868 Dome, Marine Chemistry, https://doi.org/10.1016/j.marchem.2014.09.009, 2014.

869 Crameri, F.: Scientific colour maps, , https://doi.org/10.5281/ZENODO.1243862, 2023.

870 Cullen, J. T.: On the nonlinear relationship between dissolved cadmium and phosphate in the
871 modern global ocean: Could chronic iron limitation of phytoplankton growth cause the kink?,
872 Limnology and Oceanography, 51, 1369–1380, https://doi.org/10.4319/lo.2006.51.3.1369, 2006.

873 Cullen, J. T. and Sherrell, R. M.: Effects of dissolved carbon dioxide, zinc, and manganese on
874 the cadmium to phosphorus ratio in natural phytoplankton assemblages, Limnology and
875 Oceanography, 50, 1193–1204, https://doi.org/10.4319/lo.2005.50.4.1193, 2005.

876 Cullen, J. T., Lane, T. W., Morel, F. M. M., and Sheerell, R. M.: Modulation of cadmium uptake
877 in phytoplankton by seawater CO2 concentration, Nature, https://doi.org/10.1038/46007, 1999.

878 Cullen, J. T., Chase, Z., Coale, K. H., Fitzwater, S. E., and Sherrell, R. M.: Effect of iron
879 limitation on the cadmium to phosphorus ratio of natural phytoplankton assemblages from the
880 Southern Ocean, Limnology and Oceanography, https://doi.org/10.4319/lo.2003.48.3.1079,
881 2003.

882 Cutter, G. A. and Bruland, K. W.: Rapid and noncontaminating sampling system for trace
883 elements in global ocean surveys, Limnology and Oceanography: Methods,
884 https://doi.org/10.4319/lom.2012.10.425, 2012.

885 Das, P., Samantaray, S., and Rout, G. R.: Studies on cadmium toxicity in plants: A review,
886 https://doi.org/10.1016/S0269-7491(97)00110-3, 1997.

887 DiTullio, G. R. and Smith, W. O.: Relationship between dimethylsulfide and phytoplankton
888 pigment concentrations in the Ross Sea, Antarctica, Deep-Sea Research Part I,
889 https://doi.org/10.1016/0967-0637(95)00051-7, 1995.

890 DiTullio, G. R., Geesey, M. E., Leventer, A., and Lizotte, M. P.: Algal pigment ratios in the Ross
891 Sea: Implications for Chemtax analysis of Southern Ocean data, 35–51,
892 https://doi.org/10.1029/078ARS03, 2003.

893 DiTullio, G. R., Garcia, N., Riseman, S. F., and Sedwick, P. N.: Effects of iron concentration on
894 pigment composition in Phaeocystis antarctica grown at low irradiance, Biogeochemistry, 83,
895 71–81, https://doi.org/10.1007/s10533-007-9080-8, 2007.

896 Fitzwater, S. E., Johnson, K. S., Gordon, R. M., Coale, K. H., and Smith, W. O.: Trace metal
897 concentrations in the Ross Sea and their relationship with nutrients and phytoplankton growth,

Deep-Sea Research Part II: Topical Studies in Oceanography, 47, 3159–3179, https://doi.org/10.1016/S0967-0645(00)00063-1, 2000.

Gerringa, L. J. A., Alderkamp, A.-C., van Dijken, G., Laan, P., Middag, R., and Arrigo, K. R.: Dissolved Trace Metals in the Ross Sea, Frontiers in Marine Science, 7, https://doi.org/10.3389/fmars.2020.577098, 2020.

Giordano, R., Lombardi, G., Ciaralli, L., Beccaloni, E., Sepe, A., Ciprotti, M., and Costantini, S.: Major and trace elements in sediments from Terra Nova Bay, Antarctica, Science of The Total Environment, 227, 29–40, https://doi.org/10.1016/S0048-9697(98)00402-1, 1999.

Haas, C. E., Rodionov, D. A., Kropat, J., Malasarn, D., Merchant, S. S., and de Crécy-Lagard, V.: A subset of the diverse COG0523 family of putative metal chaperones is linked to zinc homeostasis in all kingdoms of life, BMC Genomics, 10, 470, https://doi.org/10.1186/1471-2164-10-470, 2009.

Hopwood, M. J., Carroll, D., Höfer, J., Achterberg, E. P., Meire, L., Le Moigne, F. A. C., Bach, L. T., Eich, C., Sutherland, D. A., and González, H. E.: Highly variable iron content modulates iceberg-ocean fertilisation and potential carbon export, Nature Communications 2019 10:1, 10, 1–10, https://doi.org/10.1038/s41467-019-13231-0, 2019.

Horner, T. J., Lee, R. B. Y., Henderson, G. M., and Rickaby, R. E. M.: Nonspecific uptake and homeostasis drive the oceanic cadmium cycle, Proceedings of the National Academy of Sciences, 110, 2500–2505, https://doi.org/10.1073/pnas.1213857110, 2013.

Horner, T. J., Little, S. H., Conway, T. M., Farmer, J. R., Hertzberg, J. E., Janssen, D. J., Lough, A. J. M., McKay, J. L., Tessin, A., Galer, S. J. G., Jaccard, S. L., Lacan, F., Paytan, A., Wuttig, K., and GEOTRACES–PAGES Biological Productivity Working Group Members: Bioactive Trace Metals and Their Isotopes as Paleoproductivity Proxies: An Assessment Using GEOTRACES-Era Data, Global Biogeochemical Cycles, 35, e2020GB006814, https://doi.org/10.1029/2020GB006814, 2021.

Hutchins, D. and Bruland, K.: Grazer-mediated regeneration and assimilation of Fe, Zn and Mn from planktonic prey, Mar. Ecol. Prog. Ser., 110, 259–269, https://doi.org/10.3354/meps110259, 1994.

Hutchins, D. A. and Bruland, K. W.: Fe, Zn, Mn and N transfer between size classes in a coastal phytoplankton community: Trace metal and major nutrient recycling compared, issn: 0022-2402, 53, 297–313, https://doi.org/10.1357/0022240953213197, 1995.

Hutchins, D. A., Wang, W. X., Schmidt, M. A., and Fisher, N. S.: Dual-labeling techniques for trace metal biogeochemical investigations in aquatic plankton communities, Aquatic Microbial Ecology, https://doi.org/10.3354/ame019129, 1999.

Irving, B. H. and Williams, R. J. P.: The Stability of Transition-metal Complexes, Journal of the Chemical Society (Resumed), https://doi.org/10.1039/JR9530003192, 1953.

Jackson, S. L., Spence, J., Janssen, D. J., Ross, A. R. S., and Cullen, J. T.: Determination of Mn, Fe, Ni, Cu, Zn, Cd and Pb in seawater using offline extraction and triple quadrupole ICP-MS/MS, Journal of Analytical Atomic Spectrometry, 33, 304–313, https://doi.org/10.1039/c7ja00237h, 2018.

Kato, T., Nakamura, S., and Morita, M.: Determination of Nickel, Copper, Zinc, Silver, Cadmium and Lead in Seawater by Isotope Dilution Inductively Coupled Plasma Mass Spectrometry, ANAL. SCI., 6, 623–626, https://doi.org/10.2116/analsci.6.623, 1990.

Kell, R. M., Subhas, A. V., Schanke, N. L., Lees, L. E., Chmiel, R. J., Rao, D., Brisbin, M. M. M., Moran, D. M., McIlvin, M. R., Bolinesi, F., Mangoni, O., Casotti, R., Balestra, C., Horner, T., Dunbar, R. B., Allen, A. E., DiTullio, G. R., and Saito, M. A.: Zinc stimulation of phytoplankton in a low carbon dioxide, coastal Antarctic environment, https://doi.org/10.1101/2023.11.05.565706, 5 November 2023.

Kellogg, R. M., Moosburner, M. A., Cohen, N. R., Hawco, N. J., McIlvin, M. R., Moran, D. M., DiTullio, G. R., Subhas, A. V., Allen, A. E., and Saito, M. A.: Adaptive responses of marine diatoms to zinc scarcity and ecological implications, Nature Communications 2022 13:1, 13, 1–13, https://doi.org/10.1038/s41467-022-29603-y, 2022.

Lane, E. S., Semeniuk, D. M., Strzepek, R. F., Cullen, J. T., and Maldonado, M. T.: Effects of iron limitation on intracellular cadmium of cultured phytoplankton: Implications for surface dissolved cadmium to phosphate ratios, Marine Chemistry, 115, 155–162, https://doi.org/10.1016/J.MARCHEM.2009.07.008, 2009.

Lane, T. W., Saito, M. A., George, G. N., Pickering, I. J., Prince, R. C., and Morel, F. M. M.: A cadmium enzyme from a marine diatom, Nature, 435, 42–42, https://doi.org/10.1038/435042a, 2005.

Latour, P., Wuttig, K., van der Merwe, P., Strzepek, R. F., Gault-Ringold, M., Townsend, A. T., Holmes, T. M., Corkill, M., and Bowie, A. R.: Manganese biogeochemistry in the Southern Ocean, from Tasmania to Antarctica, Limnology and Oceanography, 66, 2547–2562, https://doi.org/10.1002/lno.11772, 2021.

Lee, J. and Morel, F.: Replacement of zinc by cadmium in marine phytoplankton, Marine Ecology Progress Series, 127, 305–309, https://doi.org/10.3354/meps127305, 1995.

Lee, J. G., Roberts, S. B., and Morel, F. M. M.: Cadmium: A nutrient for the marine diatom Thalassiosira weissflogii, Limnology and Oceanography, https://doi.org/10.4319/lo.1995.40.6.1056, 1995.

Lohan, M. C., Statham, P. J., and Crawford, D. W.: Total dissolved zinc in the upper water column of the subarctic North East Pacific, Deep Sea Research Part II: Topical Studies in Oceanography, 49, 5793–5808, https://doi.org/10.1016/S0967-0645(02)00215-1, 2002.

Martin, J. H.: Glacial-interglacial CO2 change: The Iron Hypothesis, Paleoceanography, https://doi.org/10.1029/PA005i001p00001, 1990.

971 Middag, R., Baar, H. J. W., and Bruland, K. W.: The relationships netween dissolved zinc and
972 major nutrients phosphate and silicate along the GEOTRACES GA02 transect in the West
973 Atlantic Ocean, Global Biogeochemical Cycles, 33, 63–84,
974 https://doi.org/10.1029/2018GB006034, 2019.

975 Morel, F. M. M., Reinfelder, J. R., Roberts, S. B., Chamberlain, C. P., Lee, J. G., and Yee, D.:
976 Zinc and carbon co-limitation of marine phytoplankton, Nature, 369, 740–742,
977 https://doi.org/10.1038/369740A0, 1994.

978 Morel, F. M. M., Milligan, A. J., and Saito, M. A.: Marine Bioinorganic Chemistry: The Role of
979 Trace Metals in the Oceanic Cycles of Major Nutrients, in: Treatise on Geochemistry: Second
980 Edition, https://doi.org/10.1016/B978-0-08-095975-7.00605-7, 2013.

981 Morel, F. M. M., Lam, P. J., and Saito, M. A.: Trace metal substitution in marine phytoplankton,
982 Annual Review of Earth and Planetary Sciences, 48, 491–517, https://doi.org/10.1146/annurev-
983 earth-053018-060108, 2020.

984 Noble, A. E., Lamborg, C. H., Ohnemus, D. C., Lam, P. J., Goepfert, T. J., Measures, C. I.,
985 Frame, C. H., Casciotti, K. L., DiTullio, G. R., Jennings, J., and Saito, M. A.: Basin-scale inputs
986 of cobalt, iron, and manganese from the Benguela-Angola front to the South Atlantic Ocean,
987 Limnology and Oceanography, https://doi.org/10.4319/lo.2012.57.4.0989, 2012.

988 Noble, A. E., Moran, D. M., Allen, A. E., and Saito, M. A.: Dissolved and particulate trace metal
989 micronutrients under the McMurdo Sound seasonal sea ice: basal sea ice communities as a
990 capacitor for iron, Frontiers in Chemistry, 1, https://doi.org/10.3389/fchem.2013.00025, 2013.

991 Ohnemus, D. C., Rauschenberg, S., Cutter, G. A., Fitzsimmons, J. N., Sherrell, R. M., and
992 Twining, B. S.: Elevated trace metal content of prokaryotic communities associated with marine
993 oxygen deficient zones, Limnology and Oceanography, https://doi.org/10.1002/lno.10363, 2017.

994 Oldham, V. E., Chmiel, R., Hansel, C. M., DiTullio, G. R., Rao, D., and Saito, M.: Inhibited
995 Manganese Oxide Formation Hinders Cobalt Scavenging in the Ross Sea, Global
996 Biogeochemical Cycles, 35, https://doi.org/10.1029/2020GB006706, 2021.

997 Park, H., Song, B., and Morel, F. M. M.: Diversity of the cadmium-containing carbonic
998 anhydrase in marine diatoms and natural waters, Environmental Microbiology,
999 https://doi.org/10.1111/j.1462-2920.2006.01151.x, 2007.

1000 Park, H., McGinn, P. J., and Morel, F. M. M.: Expression of cadmium carbonic anhydrase of
1001 diatoms in seawater, Aquatic Microbial Ecology, https://doi.org/10.3354/ame01192, 2008.

1002 Person, R., Vancoppenolle, M., Aumont, O., and Malsang, M.: Continental and Sea Ice Iron
1003 Sources Fertilize the Southern Ocean in Synergy, Geophysical Research Letters, 48,
1004 e2021GL094761, https://doi.org/10.1029/2021GL094761, 2021.

1005 Planquette, H., Sherrell, R. M., Stammerjohn, S., and Field, M. P.: Particulate iron delivery to the
1006 water column of the Amundsen Sea, Antarctica, Marine Chemistry, 153, 15–30,
1007 https://doi.org/10.1016/j.marchem.2013.04.006, 2013.

1008 Price, N. M. and Morel, F. M. M.: Cadmium and cobalt substitution for zinc in a marine diatom,
1009 Nature, 344, 658–660, https://doi.org/10.1038/344658a0, 1990.

1010 Rapp, I., Schlosser, C., Rusiecka, D., Gledhill, M., and Achterberg, E. P.: Automated
1011 preconcentration of Fe, Zn, Cu, Ni, Cd, Pb, Co, and Mn in seawater with analysis using high-
1012 resolution sector field inductively-coupled plasma mass spectrometry, Analytica Chimica Acta,
1013 https://doi.org/10.1016/j.aca.2017.05.008, 2017.

1014 Rudge, J. F., Reynolds, B. C., and Bourdon, B.: The double spike toolbox, Chemical Geology,
1015 https://doi.org/10.1016/j.chemgeo.2009.05.010, 2009.

1016 Saito, M. A. and Goepfert, T. J.: Zinc-cobalt colimitation of *Phaeocystis antarctica*, Limnology
1017 and Oceanography, 53, 266–275, https://doi.org/10.4319/lo.2008.53.1.0266, 2008.

1018 Sedwick, P. N., Di Tullio, G. R., and Mackey, D. J.: Iron and manganese in the Ross Sea,
1019 Seasonal iron limitation in Antarctic, Journal of Geophysical Research: Oceans,
1020 https://doi.org/10.1029/2000JC000256, 2000.

1021 Sedwick, P. N., Marsay, C. M., Sohst, B. M., Aguilar-Islas, A. M., Lohan, M. C., Long, M. C.,
1022 Arrigo, K. R., Dunbar, R. B., Saito, M. A., Smith, W. O., and DiTullio, G. R.: Early season
1023 depletion of dissolved iron in the Ross Sea polynya: Implications for iron dynamics on the
1024 Antarctic continental shelf, Journal of Geophysical Research, 116, C12019,
1025 https://doi.org/10.1029/2010JC006553, 2011.

1026 Shaked, Y., Xu, Y., Leblanc, K., and Morel, F. M. M.: Zinc availability and alkaline phosphatase
1027 activity in Emiliania huxleyi: Implications for Zn-P co-limitation in the ocean, Limnology and
1028 Oceanography, 51, 299–309, https://doi.org/10.4319/lo.2006.51.1.0299, 2006.

1029 Sieber, M., Conway, T. M., de Souza, G. F., Hassler, C. S., Ellwood, M. J., and Vance, D.:
1030 Cycling of zinc and its isotopes across multiple zones of the Southern Ocean: Insights from the
1031 Antarctic Circumnavigation Expedition, Geochimica et Cosmochimica Acta,
1032 https://doi.org/10.1016/j.gca.2019.09.039, 2020.

1033 Sohrin, Y., Urushihara, S., Nakatsuka, S., Kono, T., Higo, E., Minami, T., Norisuye, K., and
1034 Umetani, S.: Multielemental determination of GEOTRACES key trace metals in seawater by
1035 ICPMS after preconcentration using an ethylenediaminetriacetic acid chelating resin, Analytical
1036 Chemistry, https://doi.org/10.1021/ac800500f, 2008.

1037 St-Laurent, P., Yager, P. L., Sherrell, R. M., Stammerjohn, S. E., and Dinniman, M. S.: Pathways
1038 and supply of dissolved iron in the Amundsen Sea (Antarctica), Journal of Geophysical
1039 Research: Oceans, 122, 7135–7162, https://doi.org/10.1002/2017JC013162, 2017.

1040 Sunda, W. G. and Huntsman, S. A.: Feedback interactions between zinc and phytoplankton in
1041 seawater, Limnology and Oceanography, 37, 25–40, https://doi.org/10.4319/lo.1992.37.1.0025,
1042 1992.

Sunda, W. G. and Huntsman, S. A.: Cobalt and zinc interreplacement in marine phytoplankton: Biological and geochemical implications, Limnology and Oceanography, 40, 1404–1417, https://doi.org/10.4319/lo.1995.40.8.1404, 1995.

Sunda, W. G. and Huntsman, S. A.: Antagonisms between cadmium and zinc toxicity and manganese limitation in a coastal diatom, Limnology and Oceanography, 41, 373–387, https://doi.org/10.4319/lo.1996.41.3.0373, 1996.

Sunda, W. G. and Huntsman, S. A.: Control of Cd Concentrations in a Coastal Diatom by Interactions among Free Ionic Cd, Zn, and Mn in Seawater, Environmental Science & Technology, 32, 2961–2968, https://doi.org/10.1021/es980271y, 1998a.

Sunda, W. G. and Huntsman, S. A.: Processes regulating cellular metal accumulation and physiological effects: Phytoplankton as model systems, Science of The Total Environment, 219, 165–181, https://doi.org/10.1016/S0048-9697(98)00226-5, 1998b.

Sunda, W. G. and Huntsman, S. A.: Effect of Zn, Mn, and Fe on Cd accumulation in phytoplankton: Implications for oceanic Cd cycling, Limnology and Oceanography, 45, 1501–1516, https://doi.org/10.4319/lo.2000.45.7.1501, 2000.

Tan, D., Xu, W., Zhu, Z., Li, S., Wu, G., and Qin, H.: Optimizing the ratio of the spike to sample for isotope dilution analysis: a case study with selenium isotopes, Acta Geochimica, https://doi.org/10.1007/s11631-019-00390-6, 2020.

Taylor, S. R. and McLennan, S. M.: The Continental Crust: Its Composition and Evolution., Blackwell Scientific Publications, Oxford, 312 pp., 1985.

Twining, B. S. and Baines, S. B.: The trace metal composition of marine phytoplankton., Annual review of marine science, 5, 191–215, https://doi.org/10.1146/annurev-marine-121211-172322, 2013.

Vance, D., Little, S. H., De Souza, G. F., Khatiwala, S., Lohan, M. C., and Middag, R.: Silicon and zinc biogeochemical cycles coupled through the Southern Ocean, Nature Geoscience, 10, 202–206, https://doi.org/10.1038/NGEO2890, 2017.

Weber, T., John, S., Tagliabue, A., and DeVries, T.: Biological uptake and reversible scavenging of zinc in the global ocean, Science, 361, 72–76, https://doi.org/10.1126/SCIENCE.AAP8532, 2018.

Wright, S. W., van den Enden, R. L., Pearce, I., Davidson, A. T., Scott, F. J., and Westwood, K. J.: Phytoplankton community structure and stocks in the Southern Ocean (30-80°E) determined by CHEMTAX analysis of HPLC pigment signatures, Deep-Sea Research Part II: Topical Studies in Oceanography, https://doi.org/10.1016/j.dsr2.2009.06.015, 2010.

Wu, J. and Boyle, E. A.: Determination of iron in seawater by high-resolution isotope dilution inductively coupled plasma mass spectrometry after Mg(OH)2 coprecipitation, Analytica Chimica Acta, 367, 183–191, https://doi.org/10.1016/S0003-2670(98)00145-7, 1998.

Wuttig, K., Townsend, A. T., van der Merwe, P., Gault-Ringold, M., Holmes, T., Schallenberg, C., Latour, P., Tonnard, M., Rijkenberg, M. J. A., Lannuzel, D., and Bowie, A. R.: Critical evaluation of a seaFAST system for the analysis of trace metals in marine samples, Talanta, https://doi.org/10.1016/j.talanta.2019.01.047, 2019.

Xu, Y., Tang, D., Shaked, Y., and Morel, F. M. M.: Zinc, cadmium, and cobalt interreplacement and relative use efficiencies in the coccolithophore Emiliania huxleyi, Limnology and Oceanography, 52, 2294–2305, https://doi.org/10.4319/lo.2007.52.5.2294, 2007.

Zhao, Y., Vance, D., Abouchami, W., and de Baar, H. J. W.: Biogeochemical cycling of zinc and its isotopes in the Southern Ocean, Geochimica et Cosmochimica Acta, https://doi.org/10.1016/j.gca.2013.07.045, 2014.